The *Shigella flexneri* effector IpaH1.4 facilitates RNF213 degradation and protects cytosolic bacteria against interferon-induced ubiquitylation

Running title:

***Shigella* IpaH1.4 inhibits host ubiquitin ligase RNF213**

Luz Saavedra-Sanchez[a], Mary S. Dickinson[a], Shruti Apte[a], Yifeng Zhang[a], Maarten de Jong[b], Samantha Skavicus[a], Nicholas S. Heaton[a], Neal M. Alto[b], and Jörn Coers[a,c,#]

[a]Department of Molecular Genetics and Microbiology, Duke University Medical Center, Durham, NC 27710, USA

[b]Department of Microbiology, University of Texas Southwestern Medical Center, Dallas, TX 75390, USA.

[c]Department of Integrative Immunobiology, Duke University Medical Center, Durham, North Carolina, USA

#Correspondent footnote: Department of Molecular Genetics and Microbiology, Duke University Medical Center, Durham, NC 27710, USA. Email: jorn.coers@duke.edu

ABSTRACT

A central signal that marshals host defense against many infections is the lymphocyte-derived cytokine interferon-gamma (IFNγ). The IFNγ receptor is expressed on most human cells, and its activation leads to the expression of antimicrobial proteins that execute diverse cell-autonomous immune programs. One such immune program consists of the sequential detection, ubiquitylation, and destruction of intracellular pathogens. Recently, the IFNγ-inducible ubiquitin E3 ligase RNF213 was identified as a pivotal mediator of such a defense axis. RNF213 provides host protection against viral, bacterial, and protozoan pathogens. To establish infections, potentially susceptible intracellular pathogens must have evolved mechanisms that subdue RNF213-controlled cell-autonomous immunity. In support of this hypothesis, we demonstrate here that a causative agent of bacillary dysentery, *Shigella flexneri,* uses the type III secretion system (T3SS) effector IpaH1.4 to induce the degradation of RNF213. *S. flexneri* mutants lacking IpaH1.4 expression are bound and ubiquitylated by RNF213 in the cytosol of IFNγ-primed host cells. Linear (M1-) and lysine-linked ubiquitylation of *S. flexneri* requires RNF213 but is independent of the linear ubiquitin chain assembly complex (LUBAC). We find that ubiquitylation of *S. flexneri* is insufficient to kill intracellular bacteria, suggesting that *S. flexneri* employs additional virulence factors to escape from host defenses that operate downstream from RNF213-driven ubiquitylation. In brief, this study identified the bacterial IpaH1.4 protein as an inhibitor of mammalian RNF213 and highlights evasion of RNF213-driven immunity as a characteristic of the human-tropic pathogen *Shigella.*

43 **INTRODUCTION**
44
45 The lymphocyte-derived cytokine IFNγ is a strong inducer of cell-autonomous immunity
46 (1). The IFNγ-inducible E3 ubiquitin ligase ring finger protein 213 (RNF213) provides
47 protection against a diverse group of intracellular pathogens that includes viruses,
48 protozoa, and bacteria (2-8). RNF213 binds to bacteria that enter the host cell cytosol.
49 Once bound to Gram-negative bacteria such as *Salmonella*, RNF213 directly
50 ubiquitylates the bacterial surface molecule, lipopolysaccharide (LPS). In addition to
51 RNF213, the linear ubiquitin chain assembly complex (LUBAC) was reported to play a
52 critical role in the ubiquitylation of cytosolic bacteria (9). Whereas LUBAC catalyzes
53 linear ubiquitin chains, the types of ubiquitin linkages deposited on bacterial surfaces by
54 RNF213 are unknown. Following ubiquitylation cytosolic bacteria can be captured by
55 ubiquitin-binding proteins and delivered into autolysosomes for degradation (3).
56 While the predominantly vacuolar pathogen *Salmonella* is susceptible to
57 RNF213-mediated cytosolic host defense (3), the cytosol-adapted Gram-negative
58 pathogen *Burkholderia thailandensis* is resistant. *B. thailandensis* escapes RNF213-
59 driven host defense in part through the secretion of the virulence factor TssM, a
60 ubiquitin esterase that removes ubiquitin from LPS on the bacterial surface (10).
61 However, whether and how other cytosolic bacterial pathogens escape from RNF213-
62 driven ubiquitylation is unknown.
63 *Shigella* spp. are the etiological agent of bacillary dysentery and a leading cause
64 of diarrheal deaths, malnutrition, and growth retardation in children (11-13). *Shigella*
65 spp. invade the intestinal epithelium, enter the host cell cytosol of infected human
66 colonic epithelial cells, and trigger an acute inflammatory response that involves the
67 secretion of IFNγ by lymphocytes (14-17). IFNγ signaling in epithelial cells induces the
68 expression of human guanylate binding protein 1 (GBP1), a defense protein that blocks
69 bacterial intracellular motility and cell-to-cell spread (18-21). To counter this potent cell-
70 autonomous immune program, *Shigella flexneri* employs its type III secretion system
71 (T3SS) to deliver the GBP1 inhibitor IpaH9.8 into the host cell cytosol. Loss of IpaH9.8
72 results in diminished *S. flexneri* virulence and a potent antibacterial host response (20-
73 23).

74 IpaH9.8 belongs to a family of T3SS effectors that contain a leucine-rich repeat
75 (LRR) domain involved in substrate recognition and a novel E3 ligase (NEL) domain
76 that transfers K48-linked ubiquitin to its bound substrate (24). K48-linked ubiquitylation
77 tags the substrate for proteasomal degradation. These IpaH proteins belong to a
78 'second wave' of T3SS effectors that are under the control of the transcriptional
79 regulator MxiE. Second wave T3SS effectors have been shown to promote host cell
80 survival, to dampen inflammation, and to counteract cell-autonomous immune programs
81 (25), yet their full repertoire of targets remains to be determined.
82 In the present work we found that the MxiE-regulated T3SS effector IpaH1.4
83 facilities the proteasomal degradation of RNF213. Remarkably, RNF213 functions
84 independent of LUBAC to promote the linear and lysine-linked ubiquitylation of *ipaH1.4*-
85 deficient *S. flexneri* mutants. We observed that ubiquitylated *S. flexneri* continued to
86 replicate inside the host cell cytosol, indicating that *S. flexneri* employs additional
87 unknown virulence mechanisms to interfere with its degradation. Thus, our study
88 demonstrates that the human enteric pathogen *S. flexneri* directly interferes with
89 RNF213 expression and also limits host defense downstream of RNF213-driven
90 ubiquitylation.
91
92

RESULTS

Deletion of *mxiE* renders *S. flexneri* susceptible to linear ubiquitylation

Previous studies identified a cell-autonomous host defense program in which mammalian cells attach linear ubiquitin (M1) to the surface of the Gram-negative pathogen *Salmonella enterica* upon bacterial spillage into the host cell cytosol (3, 9). Recently, it was reported that the cytosol-adapted pathogen *B. thailandensis* secretes a ubiquitin esterase that renders the bacteria resistant to this type of cytosolic ubiquitylation (10). We therefore hypothesized that resistance to host-driven linear ubiquitylation is a common feature of bacterial pathogens that are adapted to a cytosolic milieu. To test this concept, we monitored ubiquitylation of the professional cytosolic pathogen *Shigella flexneri* (serotype 2a, strain 257T) by immunofluorescence. We found that wildtype (WT) *S. flexneri* remained largely devoid of M1-linked ubiquitin in both alveolar A549 and colonic HT29 epithelial cell lines under both unprimed and IFNγ-primed conditions (Fig. 1A – C). In contrast to WT *S. flexneri,* a Δ*mxiE* mutant strain that has diminished expression of 'second-wave' T3SS effector proteins (26, 27), was robustly stained with anti-M1 antibodies in IFNγ-primed host cells (Fig. 1A – C). These observations indicate that *S. flexneri* uses MxiE-dependent effectors to evade an IFNγ-activated ubiquitylation pathway that targets cytosolic bacteria.

Linear and lysine-linked ubiquitin is attached to *S. flexneri* Δ*mxiE*

The ubiquitin protein contains seven lysine residues. Any of these lysine residues or the N-terminal methionine of the acceptor ubiquitin can form isopeptide bonds with the C-terminal glycine residue of the donor ubiquitin to form chains. To determine which ubiquitin linkage types are present on the surface of *S. flexneri* Δ*mxiE* bacteria, we generated A549 cells that overexpressed internally tagged ubiquitin (INT-Ub) variants, which contain only a single lysine residue or lack lysines altogether. As a ubiquitin acceptor, the lysine-less (7KR) variant can only be assembled into ubiquitin chains via its N-terminal methionine. We found that 7KR INT-Ub robustly co-localized with *S. flexneri* Δ*mxiE,* albeit with diminished efficiency compared to WT INT-Ub (Fig. 2A).

123 In addition to its incorporation into linear ubiquitin chains, 7KR ubiquitin can also
124 function as donor ubiquitin and be attached as mono-ubiquitin to a substrate or to an
125 existing ubiquitin chain as a chain terminator. To distinguish between 7KR INT-Ub
126 signals originating from linear versus mono-ubiquitylation, we generated an N-terminally
127 HA-tagged 7KR INT-Ub variant. The N-terminal tag prevents linear ubiquitylation but still
128 allows 7KR INT-Ub to be attached as mono-ubiquitin via its C-terminal carboxyl group.
129 We found that the addition of this N-terminal HA-tag significantly reduced but not
130 completely abolished the number of Δ*mxiE* bacteria decorated with 7KR INT-Ub (Fig.
131 S1). These data indicate that much of the association of 7KR INT-Ub with cytosolic
132 Δ*mxiE* bacteria is due to the formation of M1-linked linear ubiquitin chains.
133 Collectively, our data confirmed that M1-linked ubiquitin is bound to *S. flexneri*
134 Δ*mxiE* but also indicated that other additional ubiquitin linkage types are attached to
135 *mxiE*-deficient bacteria. The functional importance of these lysine-linked ubiquitin chains
136 was demonstrated by improved bacterial targeting of INT-Ub variants that can form
137 additional K27-linkages or both K27- and K63-linkages (Fig. 2A). Linkage-specific
138 antibodies against K27 and K63 confirmed that these two linkage types are present on
139 *ΔmxiE* bacteria in IFNγ-primed A549 cells (Fig. 2B-C). Staining with an antibody that
140 detects most ubiquitin linkage types (FK2) showed near complete overlap with anti-M1
141 staining (Fig. 2D-E). Because the percentage of FK2-positve but M1-negatve bacteria
142 (Fig. 2E). was much smaller than the percentage of bacteria that were K27- or K63-
143 positive (Fig. 2B-C), these data suggest that most *S. flexneri ΔmxiE* bacteria are
144 decorated with both linear and lysine-linked ubiquitin.
145
146 **The ubiquitylation of *S.flexneri ΔmxiE* is dependent on RNF213 but not LUBAC**
147 Previous work showed that the multimeric E3 ligase LUBAC can deposit M1-
148 linked ubiquitin on the surface of cytosolic *S. enterica* Typhimurium (9). Moreover,
149 *S. flexneri* secretes the MxiE-regulated effector IpaH1.4 which specifically recognizes
150 and marks the LUBAC components HOIP and HOIL-1 for proteasomal degradation (28-
151 30). Consequently, we hypothesized that LUBAC was essential for the ubiquitylation of
152 *ΔmxiE.* To test this hypothesis, we infected HOIP- and HOIL-1-deficient A549 cells
153 ($HOIP^{KO}$, $HOIL\text{-}1^{KO}$, Fig. 3A) with the *ΔmxiE* mutant under IFNγ-primed conditions.

154 Unexpectedly, deletion of either HOIP or HOIL-1, each an essential component of the
155 LUBAC complex, did not diminish linear ubiquitylation of *ΔmxiE* when compared to WT
156 cells (Fig. 3B). Similarly, the internally tagged 7KR-Ub variant decorated *S. flexneri*
157 *ΔmxiE* independent of the LUBAC component HOIP (Fig. 3C). Collectively, these data
158 demonstrate that LUBAC is dispensable for linear ubiquitylation of *ΔmxiE* bacteria in the
159 host cell cytosol of IFNγ-primed A549 cells.

160 The ubiquitin E3 ligase RNF213 was recently shown to ubiquitylate pathogen-
161 containing vacuoles (2, 4) as well as Gram-positive and Gram-negative bacteria inside
162 the host cell cytosol (3, 6, 10). Like HOIL-1, RNF213 is an IFNγ-inducible protein (Fig.
163 3A and (2, 4)). Using immunofluorescence microscopy, we detected RNF213 on the
164 surface of *ΔmxiE* but not WT bacteria in IFNγ-primed A549 as well colonic HT29 cells
165 (Fig. 3D-G). The vast majority of ubiquitylated *S.flexneri ΔmxiE* mutants (~93%) co-
166 stained with anti-RNF213 (Fig. 3G), indicative of a functional role for RNF213 in the
167 ubiquitylation of *ΔmxiE* bacteria. To directly probe for RNF213 function, we infected a
168 pool of CRISPR-generated A549 RNF213^{KO} cells (Fig. 3A) with *S. flexneri ΔmxiE* and
169 stained these IFNγ-primed cells for M1-, K27-, and K63-linked ubiquitin. We found that
170 in the absence of human RNF213, antibodies specific for M1-, K27-, and K63-linked
171 ubiquitin no longer stained the surface of *S.flexneri ΔmxiE* (Fig. 3B and 3H-I). In
172 agreement with these immunofluorescence data, both WT and lysine-less ubiquitin
173 (7KR-Ub) localized to *ΔmxiE* bacteria in WT but not in RNF213^{KO} cells (Fig. 3C).
174 Together, these data demonstrate that human RNF213 is essential for the linear and
175 lysine-linked ubiquitylation of MxiE-deficient *S. flexneri* mutants.
176

177 **Ectopic expression of *S. flexneri* virulence factors IpaH1.4 or IpaH2.5 induces**
178 **RNF213 degradation**

179 The transcription factor MxiE induces the expression of several secreted effector
180 proteins of the IpaH family that act as bacterial ubiquitin E3 ligases and tag host
181 proteins for proteasomal degradation (21, 23, 28, 29, 31-35). Since our data revealed
182 that the *S. flexneri* virulence factor MxiE blocks bacterial ubiquitylation by RNF213, we
183 hypothesized that *S. flexneri* infections induce the proteasomal degradation of RNF213
184 in a MxiE-dependent manner. To test this hypothesis, we measured RNF213 protein

levels by immunoblotting in cells that had been infected with WT or *ΔmxiE S. flexneri*. Our data revealed that RNF213 protein levels are drastically reduced upon infection with WT *S. flexneri* and that the deletion of *mxiE* partially restored RNF213 expression in infected cells (Fig. 4A). Similarly, and as reported previously (9, 28, 29), HOIP protein expression is diminished in cells infected with WT *S. flexneri* but much less so in the case of infections with *ΔmxiE S. flexneri* (Fig. 4A).

To directly test whether *S. flexneri* promote proteasomal degradation of RNF213, we conducted infections in the presence of the proteasomal inhibitor MG132. As expected, MG132 largely restored RNF213 total protein levels in *S. flexneri*-infected cells (Fig. 4B). We next tested whether a specific IpaH effector facilitates the degradation of RNF213. To this end, we transiently expressed GFP-fusion proteins of individual IpaH family members in HEK 293T cells that ectopically expressed RNF213 and measured their effects on RNF213 protein levels by immunoblotting. Our mini-screen revealed that the ectopic expression of the two closely related paralogs IpaH1.4 and IpaH2.5 were sufficient to promote RNF213 degradation in HEK 293T cells (Fig. 4C). Of note, the substrate-binding LRR domains of IpaH2.5 and IpaH1.4 are 98.9% identical in DNA sequence and were previously shown to have comparable substrate specificity and functional redundancy (28). Both IpaH1.4 and 2.5 share a highly conserved NEL E3 ubiquitin ligase domain that contains an essential catalytic cysteine residue at position 368 (29). Catalytically inactive forms of IpaH1.4 or IpaH2.5, in which Cys368 is mutated to a serine (C/S), failed to degrade RNF213 (Fig. 4D). As an additional control we included overexpression of IpaH9.8, an inhibitor of GBPs, which also did not impact RNF213 expression (Fig. 4D), as anticipated.

To investigate potential physical interactions between IpaH1.4 and IpaH2.5, we reanalyzed a previously generated dataset that employed a method known as ubiquitin-activated interaction traps (UBAITs) (32). As depicted in Fig. S2A, the human ubiquitin gene was fused to the 3′ end of IpaH2.5, producing a C-terminal IpaH2.5-ubiquitin fusion protein. When incubated with ATP, a ubiquitin-activating enzyme E1, and a ubiquitin-conjugating enzyme E2, the IpaH2.5-ubiquitin "bait" protein is capable of binding to and ubiquitylating target substrates. This ubiquitylation creates an iso-peptide bond between the IpaH2.5 bait and its substrate, thereby enabling purification via a

216 Strep affinity tag incorporated into the fusion construct (32). IpaH2.5-ubiquitin bait and
217 IpaH3-ubiquitin control proteins were incubated with lysates from murine intestinal
218 tissue. To detect interaction partners in a physiologically relevant setting, we used
219 intestinal lysates derived from mice infected with *Salmonella,* which in contrast to
220 *Shigella* causes pronounced inflammation in WT mice and therefore better simulates
221 human *Shigellosis* in an animal model. Using UBAIT we identified HOIP (Rnf31) as a
222 likely IpaH2.5 binding partner (Fig. S2B), thus confirming previous observations (28)
223 and validating the effectiveness of our approach. Strikingly, we identified mouse Rnf213
224 as the most abundant interaction partner of the IpaH2.5-ubiquitin bait protein (Fig. S2B).
225 Collectively, our data and concurrent reports showing direct interactions between
226 IpaH1.4 and human RNF213 (36, 37) indicate that the virulence factors IpaH1.4 and
227 IpaH2.5 directly bind and degrade mouse as well as human RNF213.
228
229 **Loss of IpaH1.4 is sufficient to render *S. flexneri* susceptible to RNF213-driven**
230 **ubiquitylation in human and murine host cells**
231 Given that ectopic expression of either IpaH1.4 or IpaH2.5 was sufficient to
232 degrade RNF213, we expected these two endogenous effectors to be functionally
233 redundant. However, we found that genetic deletion of *ipaH1.4* in either *S. flexneri*
234 serotype 2a strain 257T (Fig. 5A-B) or in serotype 5a strain M90T (Fig. S3A) was
235 sufficient to restore RNF213 protein expression and RNF213 recruitment to cytosolic
236 bacteria. A deletion mutant of *ipaH2.5* was as resistant to RNF213 targeting as co-
237 isogenic WT bacteria and a Δ*ipaH1.4-ipaH2.5* double mutant was indistinguishable from
238 the Δ*ipaH1.4* single deletion mutant (Fig. S3A). These data suggested that endogenous
239 IpaH2.5 is non-functional, which agrees with a previous characterization of *ipaH2.5* as a
240 minimally expressed pseudogene (38).
241 Previous work showed that IpaH1.4 binds to and degrades the LUBAC subunit
242 HOIP (9, 28, 29). To determine whether the degradation of RNF213 could be indirect
243 and HOIP-dependent, or vice versa, we monitored RNF213 expression in HOIP^{KO} cells
244 and HOIP expression in RNF213^{KO} cells. We found that expression of RNF213
245 remained at WT levels in the absence of HOIP and that the degree of IpaH1.4-
246 dependent RNF213 degradation was comparable in WT and HOIP^{KO} cells (Fig. 5A).

247 Similarly, infections with WT but not Δ*ipaH1.4* mutant *S. flexneri* resulted in a substantial
248 reduction of HOIP protein expression in RNF213^{KO} cells (Fig. S3B). These observations
249 show that IpaH1.4 targets RNF213 and HOIP for degradation independent from each
250 other.

251 The sustained RNF213 expression in cells infected with *S. flexneri* Δ*ipaH1.4* (Fig.
252 5A) correlated with staining of cytosolic Δ*ipaH1.4* bacteria with RNF213 (Fig. 5B-C). As
253 expected, the complementation of the Δ*ipaH1.4* mutant with WT IpaH1.4 efficiently
254 prevented RNF213 recruitment to cytosolic bacteria, whereas complementation with
255 catalytically inactive IpaH1.4 did not (Fig. 5C-D). Through the use of linkage-specific
256 antibodies, we also observed M1-, K27-, and K63-linked ubiquitin on cytosolic Δ*ipaH1.4*
257 bacteria in IFNγ-primed WT A549 cells (Figs. 5E, S3C-E). In contrast to IFNγ-primed WT
258 A549 cells, IFNγ-primed RNF213^{KO} A549 cells lacked linear ubiquitylation of Δ*ipaH1.4*
259 (Fig. 5E). This ubiquitylation of *S. flexneri* Δ*ipaH1.4* was independent of LUBAC, as it
260 occurred in HOIL-1^{KO}, HOIP^{KO}, and WT A549 cells at comparable frequencies (Fig.
261 S3F).

262 Although *S. flexneri* is a human-adapted pathogen, some IFNγ-inducible host
263 defense programs targeting *S. flexneri* and the corresponding bacterial evasion
264 mechanisms transcend host barriers. For example, the *Shigella* virulence factor IpaH9.8
265 inhibits both human and murine guanylate binding proteins (GBPs) (23, 39). We
266 therefore asked whether RNF213 ubiquitylates *S. flexneri ΔipaH1.4* in at least one other
267 mammalian species, the mouse. To do so, we infected unprimed and IFNγ-primed WT
268 and Rnf213^{KO} mouse embryonic fibroblasts (MEFs, Fig. S4A) with *S. flexneri* WT and
269 *ΔipaH1.4* mutant. We observed that *ΔipaH1.4* bacteria became decorated with mouse
270 Rnf213 (Fig. S4B) and linear ubiquitin chains (Fig. S4C). The IFNγ-dependent increase
271 in the percentage of M1-ubiquiitn decorated *ΔipaH1.4 S. flexneri* bacteria was reversed
272 in *Rnf213*^{KO} MEFs (Fig. S3C). Collectively, these data depict a conserved role for the
273 mammalian ubiquitin E3 ligase RNF213 in cytosolic immune surveillance and
274 demonstrate that IpaH1.4 can evade both mouse and human RNF213-driven linear
275 ubiquitylation.

276 Ubiquitylated microbial cargo can be delivered into microbicidal lysosomes in an
277 autophagy-like process commonly referred to as xenophagy (40). Previous work
278 showed that linear ubiquitylation of *S. enterica* leads to bacterial clearance by
279 xenophagy (3). In contrast to the xenophagic killing of ubiquitylated *S. enterica,* we
280 found that ubiquitylated *S. flexneri ΔIpaH1.4* and *ΔmxiE* mutant bacteria continued to
281 replicate inside IFNγ-primed A549 cells (Fig. 5H), reminiscent of the continued growth of
282 ubiquitylated *B. thailandensis tssM* mutants inside the host cell cytosol of human IFNγ-
283 primed cells (10). Thus, our data indicate that *S. flexneri*, like *B. thailandensis,* can block
284 ubiquitin-dependent xenophagy both at the stage of ubiquitylation and at another so far
285 undetermined downstream step of this cell-autonomous host defense pathway.

286 **DISCUSSION**

287 Xenophagy is a cell-autonomous defense program in which intracellular pathogens are
288 captured and delivered into degradative lysosomes. Ubiquitylation of intracellular
289 pathogens is the most common initiating step for xenophagy (40). Like other steps of
290 the xenophagy cascade, pathogen ubiquitylation is augmented in cells primed with the
291 lymphocyte-derived cytokine IFNγ (2, 4, 7, 41, 42). An antimicrobial E3 ubiquitin ligase,
292 RNF213, is itself an IFNγ-inducible protein (2-7). Here, we report that the enteric human
293 pathogen *S. flexneri* employs the T3SS effector IpaH1.4 to induce the proteasomal
294 degradation of RNF213. Accordingly, loss of IpaH1.4 results in RNF213-depdendent
295 ubiquitylation of *S. flexneri*. However, IpaH1.4-deficient *S. flexneri* mutants, despite their
296 ubiquitylation, continue to replicate inside the cytosol of IFNγ-primed human cells.
297 These observations suggest that *S. flexneri* not only evades RNF213-driven
298 ubiquitylation but also the downstream degradation of ubiquitylated bacteria.

299 Accompanying previous reports on *Chlamydia* and *Burkholderia* (4, 10), our
300 study on *Shigella* provides evidence that host-adapted intracellular pathogens escape
301 from RNF213-driven host defense. Each of these pathogens evolved a mechanistically
302 distinct strategy to escape ubiquitylation by RNF213. The soil-dwelling accidental
303 pathogen *B. thailandensis* is recognized and ubiquitylated by RNF213 but instantly
304 removes ubiquitin from its surface through the activity of its secreted ubiquitin esterase
305 TssM (10). The human pathogen *Chlamydia trachomatis* decorates its surrounding
306 vacuole with the secreted T3SS effector GarD, which renders the *Chlamydia*-containing
307 vacuole invisible to RNF213 (4). In contrast to TssM and GarD, the *Shigella* effector
308 IpaH1.4 is a direct inhibitor of RNF213, which is further supported by recently published
309 biochemical studies demonstrating direct interactions between the LRR domain of
310 IpaH1.4 and the RING domain of RNF213 (36, 37).

311 IpaH1.4 and IpaH2.5 have nearly 99% sequence identity in their substrate-
312 binding LRR domains and overexpression of either paralog is sufficient to trigger
313 RNF213 degradation. However, only IpaH1.4 appears to be essential for *S. flexneri*-
314 triggered RNF213 degradation – as shown in the present work – or for HOIP
315 degradation (28). While these observations agree with a previous report demonstrating
316 low expression of IpaH2.5 under standard culture conditions (38), it remains to be seen

317 whether IpaH2.5 is expressed and possibly redundant with IpaH1.4 for virulence during
318 *in vivo* infections.

319 The mechanism by which IpaH1.4 and its paralog IpaH2.5 promote RNF213
320 degradation can be gleaned from previous studies characterizing IpaH1.4 and IpaH2.5
321 as ubiquitin E3 ligases that directly conjugate K48-linked ubiquitin to the LUBAC subunit
322 HOIP leading to HOIP degradation by the proteasome (28). Indeed, studies published
323 during the revisions of our manuscript show that IpaH1.4 and IpaH2.5 similarly bind to
324 and directly ubiquitylate RNF213 to facilitate RNF213's proteasomal degradation (36,
325 37). Such direct interactions are additionally supported by our data showing that
326 transient IpaH2.5-RNF213 interactions can be trapped via formation of covalent bonds
327 between these proteins in a UBAIT assay.

328 The deletion of *ipaH1.4* leads to *S. flexneri* ubiquitylation in IFNγ-primed host
329 cells. Different ubiquitin linkage types and their incorporation into heterotypic conjugates
330 create a rich diversity of ubiquitin modifications with unique functional outputs, which is
331 commonly referred to as the 'ubiquitin code.' (43, 44). We found that at least three
332 linkage types are attached to *S. flexneri* Δ*ipaH1.4* in an RNF213-dependent manner:
333 K27, K63, and linear (M1). Linear ubiquitylation is a head-to-tail inter-ubiquitin linkage
334 through the amino group of the N-terminal methionine (M1) and the C-terminal carboxyl
335 group (45). The LUBAC complex is the only recognized ubiquitin E3 ligase able to
336 conjugate M1-linked ubiquitin chains (46, 47). However, we observed that LUBAC is
337 dispensable for M1-linked ubiquitylation of cytosolic *S. flexneri* Δ*ipaH1.4.* We found that
338 lysine-less internally tagged ubiquitin or an M1-specific antibody bound to *S. flexneri*
339 Δ*ipaH1.4* in cells lacking LUBAC (HOIL-1^{KO} or HOIP^{KO}) but failed to bind bacteria in
340 RNF213-deficient cells. These data corroborate our previous observations, which
341 suggested that IFNγ-induced linear ubiquitylation of *Chlamydia*- and *Toxoplasma*-
342 containing vacuoles occur independent of LUBAC in human cells (2, 4). While RNF213
343 itself may catalyze such linear ubiquitin conjugation, it is equally possible that this
344 reaction is carried out by additional ubiquitin E3 ligases that are being recruited to the
345 bacterial surface alongside RNF213.

346 It was previously reported that RNF213 ubiquitylates LPS on the surface of
347 *S. enterica* prompting the recruitment of LUBAC, which catalyzes the conjugation of

348 linear ubiquitin to the surface of *S. enterica* (3). Whereas LUBAC was found to be
349 essential for M1-linked ubiquitylation of cytosolic *S. enterica* (9), we find that LUBAC is
350 dispensable for M1-linked ubiquitylation of *S. flexneri* Δ*ipaH1.4* bacteria. While
351 differences between *S. enterica* and *S. flexneri,* for example in the composition of their
352 bacterial cell walls, could possibly contribute to these discrepant results, it is also
353 important to note that the previous *S. enterica* infection studies were conducted in naïve
354 cells (3, 9), whereas our studies were performed under IFNγ priming conditions. We
355 therefore propose that a boost in the expression of RNF213 and other IFN-stimulated
356 genes (ISGs) renders LUBAC obsolete for M1-linked ubiquitylation of Gram-negative
357 bacteria. Future studies are needed to determine how RNF213 co-operates with LUBAC
358 and other host factors to ubiquitin-tag intracellular pathogens.
359 *Shigella* is a human adapted pathogen that secretes T3SS effectors to directly
360 interfere with type I and III IFN signaling in epithelial cells (48). Additionally, *Shigella*
361 employs virulence factors that inhibits ISGs which act downstream from IFN signaling.
362 For example, the T3SS effector IpaH9.8 blocks the activity of IFNγ-inducible
363 antimicrobial ISGs such as GBP1 (20-23). Here we report that IpaH1.4 inactivates
364 another ISG, *i.e.* RNF213. Because ubiquitylated *S. flexneri* Δ*ipaH1.4* and Δ*mxiE*
365 mutants continue to replicate inside the cytosol of IFNγ-primed host cells, we propose
366 that *S. flexneri* also uses a mxiE-independent T3SS effector to interfere with host
367 defenses occurring downstream from RNF213. Collectively, these data indicate that
368 *Shigella* is equipped with redundant counter-immune mechanisms. This type of bacterial
369 effector redundancy is not unique to *Shigella*. It was recently shown that the rodent
370 pathogen *Citrobacter rodentium* can tolerate various combinations of individual T3SS
371 effector deletions *in vivo,* an observation that led to the 'T3SS effector networks'
372 hypothesis (49, 50). Further characterization of the *Shigella* T3SS effector network that
373 renders bacteria resistant to IFNγ-inducible cell-autonomous immune program will
374 provide a deeper understanding of the pathogenesis of this important human enteric
375 pathogen. Given the rise of extensively drug-resistant *Shigella* strains (51-54), such an
376 understanding may prove to be essential for the development of critically needed novel
377 therapeutic approaches to treat Shigellosis.
378

379

380 **MATERIALS AND METHODS**

381

382 **Cell culture**

383 A549 (ATCC #CCL-185), HT-29 (ATCC #HTB-38), and mouse embryonic fibroblasts
384 (MEFs) were cultured in Dulbeco's Modified Eagle Medium (DMEM, Gibco)
385 supplemented with 1% MEM non-essential aminoacids (Gibco), 55 uM 2-
386 Mercaptoethanol (Gibco) and 10% heat inactivated fetal bovine-serum. MEFs were
387 generated from E12- E14 embryos as previously described (55). Cells were grown at 37
388 °C in 5% $C0_2$. Cell lines were authenticated using GenePrint10 (Promega) by the Duke
389 University DNA Analysis Facility. All cell lines were routinely tested for mycoplasma.

390

391 **Knock out cell lines and mammalian expression systems**

392 The production and characterization of A549 knockout cell lines (pooled RNF213KO,
393 $HOIP^{KO}$ clone and $HOIL\text{-}1^{KO}$ clone) was previously reported (2, 4). Various GFP-tagged
394 IpaH expression constructs including the IpaH1.4 and IpaH2.5 C/S mutants were
395 previously described (28). Internally Strep-tagged ubiquitin (INT-Ub) and Internally
396 Strep-tagged & N-Terminally HA-tagged ubiquitin (NTerm-HA-Ub_ INT-Strep) open
397 reading frames were cloned via Gateway cloning into the lentiviral expression plasmid
398 pLEX307, a gift from Dr. David Root (Addgene plasmid # 41392;
399 http://n2t.net/addgene:41392; RRID: Addgene_41392). DNA of full length human
400 RNF213 with N-terminal mCherry was a gift from Daisuke Morito (56). RNF213 was
401 amplified in segments using PCR and cloned using Golden Gate assembly with the
402 enzyme kit BsmBI-v2 (New England Biolabs). Endogenous BsmBI sites were removed
403 from RNF213 by introducing silent mutations in primers used to add enzyme overhangs
404 for Golden Gate assembly. RNF213 was first cloned into a modified Gateway donor
405 vector pDONR221 (Thermo Fisher Scientific) containing a golden gate cloning site in
406 between ATTP sites to make pENTR-mCherry-RNF213. mCherry-RNF213 was
407 transferred into piggybac vector PB-TA-ERN using LR clonase enzyme (Thermo Fisher
408 Scientific) for dox-inducible expression of mCherry-RNF213. PB-TA-ERN (57) was a gift
409 from Knut Woltjen (Addgene plasmid #80474; http://n2t.net/addgene:80474; RRID:
410 Addgene_80474). Whole plasmid sequencing of PB-TA-ERN-mCherry-RNF213 and the

411 INT-Ub vectors was performed by Plasmidsaurus using Oxford Nanopore Technology
412 with custom analysis and annotation. The INT-Ub protein sequences are provided in
413 table 1 in supplemental material. For mCherry-RNF213 expression in human cells,
414 293T cells (ATCC CRL-3216) were transfected with PB-TA-ERN and piggybac
415 transposase (pRP[Exp]-EGFP-EF1A>hyPBase, VectorBuilder) using lipofectamine 2000
416 transfection reagent (Thermo Fisher Scientific), according to manufacturer's
417 instructions. Cells were grown for approximately 8 days to allow for loss of the
418 transiently transfected vectors, while mCherry-RNF213 that had integrated into the
419 293T genome was being maintained.
420

421 **Production of Rnf213 knockout mouse and derived cells**

422 RNF213 knockout mice were generated using a modified iGONAD methodology (58-
423 60). Briefly, 1-day time mated, vaginal-plug-positive 8 – 24-week-old C57BL/6J female
424 mice were put under isoflurane anesthesia. A dorsal surgical incision was made, and the
425 ovary/oviduct was exposed. The oviduct was injected with a 0.5 µL Cas9/CRISPR mix
426 which included 6.1 µM Cas9 protein (IDT, Cat. #1081058), 30 µM sgRNAs (IDT, Alt-R
427 CRISPR-Cas9 sgRNA), and 0.02% Fast Green FCF (VWR, Cat. #AAA16520-14) in
428 Opti-MEM (Thermo Fisher Scientific, Cat. #11058021). The 30 µM sgRNA concentration
429 included the following two sgRNAs targeting exon 28 of Rnf213: 5'-
430 TTAAATACTGGTAAGGTCGT(TGG)-3' and 5'-AGTCGGAGTAGCAAAATCCC(TGG)-3'.
431 After the Cas9/sgRNA mix injection, the oviducts were covered with tissue and then
432 electroporated using a CUY21EDIT II (BEX Co., Ltd.) electroporator with the settings:
433 Square mA mode, Pd V: 60 V, Pd A: 100 mA, Pd on: 5 ms, Pd off: 50 ms, Pd N: 3, and
434 Decay: 10%. This procedure was done on both set of oviducts in the mouse. After
435 surgery, female mice were housed together and at 19-21 days post-surgery monitored
436 for pup birth. Pups were genotyped and three founder mice with out-of-frame 101 bp,
437 284 bp, or 407 bp deletions within exon 28, respectively, were selected and bred to
438 homozygosity. Loss of Rnf213 protein expression in cells derived from these knockout
439 mice was validated by Western blotting.
440

441 **Lentivirus production**

442 Plasmids were transfected into HEK 293T cells using the TransIT 293 transfection
443 reagent (Mirus). Wells were transfected with 1ug plasmid, 750 ng pGAGpol, 250 ng
444 VSVG. 6 hours post transfection, media was aspirated and replaced with fresh DMEM.
445 24 hours post transfection, media was aspirated and replaced with pseudoparticle
446 DMEM (3%fbs, 1% MEM non-essential aminoacids, 20mM HEPES). Supernatant was
447 collected 48 and 72 hours after transfection. Supernatants containing lentivirus were
448 filtered using 0.45um filters (corning) and later mixed with 10ug/ml polybrene (Millipore
449 Sigma). Virus was frozen at -80 until use. For cell transduction, A549 cells were diluted
450 to a concentration of 3.33 x 10^4 cells/ml and mixed with 10 ug/ml polybrene. 500 µl of
451 lentivirus was added to each well of a 6 well plate, and 1.5 ml of diluted cells were
452 added on top. Cells were selected in media with 1µg/ml of puromycin and expanded.
453
454 **IpaH mini-screen**
455 HEK 293T that express PiggyBac RNF213 were seeded at 10^5 cells/well. Sixteen hours
456 before transfection, aTc was added to cells to induce expression of RNF213. The next
457 morning, 2.5 µg of IpaH effector-encoding plasmids were used to transfect HEK 293T
458 using the TransIT 293 transfection reagent (Mirus). 24 hours after transfection, cells
459 were lysed in RIPA buffer and prepared for immunoblotting, as described (20).
460
461 **Bacterial strains**
462 All *S. flexneri* strains were grown on Tryptic Soy Broth (TSB, Millipore Sigma) agar
463 plates in presence of 0.01% of Congo Red (Millipore Sigma) and red colonies were
464 cultured in TSB broth culture. *S. flexneri* 2457T wildtype and mutant strains (*ΔmxiE and*
465 *ΔipaH1.4*) were previously described (20). *S. flexneri* M90T strains (wildtype, *ΔipaH2.5,*
466 *ΔipaH1.4 and* ∆*ipaH1.4-ipaH2.5*) were also previously reported (28). For
467 immunofluorescence studies, we used fluorescent *S. flexneri* strains carrying the
468 pGFPmut2 (61) or the pJUMP45-2A (sfGFP) (62) plasmids. Bacteria were transformed
469 with the ilux pGEX() plasmid (Addgene plasmid #107879) (63) to generate
470 bioluminescent bacteria, as previously reported (64). Where specified, *S. flexneri*.
471 strains were used that harbor the pilT plasmid which encodes an adhesin (65) and
472 enhances bacterial adhesion to host cells. To complement the *ΔipaH1.4* strain, full

473 length IpaH1.4 and its catalytically inactive variant C368S were cloned into the bacterial
474 expression vector pDSW206 using Takara In-Fusion Snap Assembly Master Mix (Cat#
475 638948) following the manufacturer's instructions. Bacterial transformation was
476 performed as previously described (20). Antibiotics were used as needed at the
477 following concentration: carbenicillin (50 ug/ml), kanamycin (50 ug/ml), spectinomycin
478 (50ug/ml), and chloramphenicol (100 ug/ml).
479
480 **Infection procedures**
481 For immunofluorescence staining A549, HT29, and MEF cells were seeded at $1x10^5$
482 cells per well on cover slips in 24-well plates. HT29 cells were plated at $2x10^5$ cells per
483 well. For Western blotting cells were plated at $2x10^5$ cells per well in 24-well plates.
484 Cells were either left untreated or treated overnight with human or mouse cytokine IFNγ
485 at a final concentration of 100 U/ml, as indicated. The day before infection, *S. flexneri*
486 was inoculated into TSB with antibiotics as needed and grown overnight at 37°C with
487 aeration. The next day bacteria were diluted (1:20) in TSB with antibiotics and grown for
488 1h 30 minutes. To induce the expression of WT and C368S mutant IpaH1.4 in
489 complemented *ΔipaH1.4* bacteria*,* 1mM IPTG (Invitrogen 15529-019) was added 1 hour
490 after subculturing. Subsequently, the optical density of the broth culture was measured
491 and pelleted bacteria were washed in sterile PBS and resuspended in DMEM. Infections
492 were carried out at an approximate multiplicity of infection (MOI) of 50 to 100, unless
493 otherwise specified. Cells were centrifuged at 1000 g for 10 minutes at the time of
494 infection and infected cells were incubated at 37°C with 5% CO_2. Cells were washed
495 with warm HBSS two times after 90 minutes (A549 and HT29 cells) or 60 minutes
496 (MEFs) post infection. Following these washes gentamicin at a final concentration of 50
497 ug/ml (for A549 and MEFs) or 100 ug/ml (for HT29) was added to the media. For
498 fluorescence microscopy infected cells were fixed with 4%PFA in phosphate-buffered
499 saline (PBS) at 4 hpi (A549 cells), 3 hpi (HT29), or 2 hpi (MEFs). All *S. flexneri* strains
500 carried the plasmid pGFPmut2 to visualize bacteria by fluorescence microscopy. For
501 Western blotting, bioluminescence experiments, and MEF infections, *S. flexneri* strains
502 expressed PilT for improved adhesion and infection rates.
503

504 **Immunofluorescence microscopy**

505 Cells were fixed in 4% PFA in PBS and then permeabilized either with 0.1%triton in PBS
506 for 15 minutes or with ice-cold methanol for 1 minute followed by 0.05% saponin in
507 blocking buffer. Blocking buffer was composed of 5% BSA, 2.2% glycine +/- 0.05%
508 saponin or 10% goat serum and 0.05 % saponin in PBS. Following permeabilization,
509 coverslips were blocked for 30 minutes at room temperature (RT). Next, coverslips were
510 incubated with the respective primary antibody diluted in blocking buffer overnight at
511 4°C. The following primary antibodies were used: rabbit monoclonal anti-RNF213
512 (Sigma HPA026790; 1:1000), rabbit monoclonal anti-linear (M1) ubiquitin; clone 1E3
513 (Sigma ZRB2114; 1:250), mouse polyclonal anti-ubiquitin FK2 (Cayman Chemical
514 14220; 1:100), rabbit monoclonal anti-K63 ubiquitin, clone Apu3 (Sigma 05-1308.
515 1:100), rabbit monoclonal anti K27 (Abcam ab181537, 1:100), mouse monoclonal anti-
516 Strep (Genscript A01732, 1:200), custom rabbit anti-mRnf213 antibody from an animal
517 immunized with peptides RKSNEGGNTQPEDQRKPGEGR (aa296-316) and
518 KDTVEYEFIYEQAQKKGE (aa429-446) (Life Technologies, 1:100). Coverslips were
519 then washed three times with 0.05% Triton in PBS or 0.05% saponin and incubated with
520 an Alexa Fluor-conjugated secondary antibody (1:1000, Invitrogen) and nuclear dye
521 Hoechst 33258 (2ug/ml; Invitrogen) for 1 hour at RT. Next, coverslips were washed
522 three times with 0.05% Triton or 0.05% saponin in PBS and mounted on glass slides
523 using a mix of with mowiol 4-88 combined with para-phenylenediamine antifading agent
524 (9:1). Coverslips were imaged at a Zeiss Axio Imager microscope with Apotome 3 using
525 a 63×/1.4 NA Oil immersion lens. Two to eleven fields of view were captured per
526 coverslip to account for at least 100 bacteria, and z slices with an interval of 0.5 µm
527 were taken per field of view. Images were processed on the software program Fiji.
528 Bacteria that had protein signal surrounding at least 50% of its visible surface were
529 considered as targeted.

530

531 **Bacterial luminescence assay**

532 Infections were conducted with bacterial strains carrying the pilT plasmid to promote cell
533 adhesion and the ilux plasmid as a bioluminescence reporter. Host cells were seeded in
534 96-well plates at a density of 2.5 x10^4 cells per well. An approximate MOI of 5 in an

535 infection volume of 100 µl per well was used. Twenty-five minutes post infection, wells
536 were washed once with 200 µl of warm HBSS and then fresh DMEM containing 50µg
537 /ml gentamicin was added to each well. Bacterial bioluminescence was measured on a
538 multimode microplate reader (Biotek Synergy H1, Agilent) every 30 minutes, starting at
539 1 hpi and finishing at 8 hpi.
540
541 **Western blotting**
542 After infection, cells were washed two times with cold HBSS and lysed in RIPA buffer
543 (Sigma) in the presence of 4U/ml DNAse I (NEB) and protease inhibitor cocktail
544 (Sigma). Lysates were incubated at 4°C for 30 min and centrifuged at 20,000g for 12
545 minutes at 4°C. Protein concentrations were measured using the BCA kit (Thermofisher)
546 and normalized. Normalized samples were mixed with Laemmli buffer that contained
547 5% β- mercaptoethanol and heated at 95°C for 10 minutes. Sample were heated at 56
548 °C for 10 minutes when samples were prepared for RNF213 immunoblotting. Ten to
549 thirty µg of protein sample were resolved on a 4-20% Mini-Protean TGX stain-free gels
550 (Biorad) and then blotted onto a PVDF membrane using a tank transfer system
551 overnight at 4°C. After the transfer, PVDF membranes were blocked with 5% nonfat dry
552 milk in Tris-buffered saline containing 0.1%Tween20 (Sigma-Aldrich) (TBS-T) for 1 hour
553 at RT. Subsequently, membranes were incubated with primary antibody diluted in
554 blocking solution overnight at 4°C. After primary antibody incubation, blots were washed
555 three times with TBST and incubated with the respective secondary antibody in blocking
556 solution for 1 hour at RT. Afterwards, membranes were washed with TBS-T and
557 developed with Clarity ECL (Cytiva). Blots were imaged on an Azure 500 visualization
558 system. Primary antibodies used in this study include rabbit monoclonal anti-RNF213
559 (Sigma HPA026790 1:2000), rabbit polyclonal anti-GAPDH (Abcam ab9845; 1:10000);
560 mouse monoclonal anti HOIL-1, clone E3E (Sigma MABC576; 1:500); custom rabbit
561 anti-mRnf213 (Life Technologies, 1:500); rabbit polyclonal anti-HOIP (Abcam ab46322;
562 1:500); monoclonal Anti-β-Actin (Sigma A2228, 1:6000). Images were processed in Fiji.
563
564 **UBAIT Substrate Capture Assays.**

565 UBAIT assays were performed essentially as described before (32). Briefly, unknown
566 substrates were captured from colon and cecum lysates from 6-8 weeks old wild type
567 C57BL/6 (Charles River) mice. All mouse infection experiments conducted were in
568 accordance with the policies of the Institutional Animal Care and Use Committee at UT
569 Southwestern. Mice were orally infected by gavage with $1x10^9$ *Salmonella enterica*
570 Typhimurium S1344 WT and after 4 days mice were euthanized and colon and cecum
571 were removed, washed and homogenized in Lysis Buffer (1x Ubiquitination buffer
572 (Boston Biochem), 1x protease inhibitor (Sigma), 1mM DTT). Homogenates were then
573 centrifuged at 13,000g at 4˚C for 10 minutes and supernatants were added to UBAIT
574 reactions. The supernatant were incubated with 25 ug of purified Strep-IpaH2.5-
575 3xFLAG-Ub or Strep-IpaH3-3xFLAG-Ub and rotated at 4˚C. After 1 hour, His-UbE1
576 (100nM), His-UbcH5b (2000nM), energy regeneration buffer (Boston Biochem), MgCl
577 (1mM) and 1 x ubiquitination buffer were added to a final volume of 500 µl. The reaction
578 was run at 30˚C for 10 minutes and then 300 µl TBS buffer (25 mM Tris-HCL pH7.4, 150
579 mM NaCl, 1mM DTT) and 30 µl of washed Strep-Tactin Superflow beads (Iba
580 LifeSciences) were added and rotated for 2 hours at 4˚C. The beads were washed 4
581 times in TBS-T (TBS+ 0.5% Triton-X100) and 2 times in TBS. Strep-IpaH2.5-3xFLAG-
582 Ub was eluted from the beads in 150 µl Strep-tag elution buffer (Iba LifeSciences).
583 Eluted sample and beads were centrifuged, and supernatant moved to a new tube. SDS
584 (0.25% final concentration) and DTT (5mM final concentration) were added, and
585 samples were heated at 95˚C for 5 minutes. Next, 1.2 ml TBS was added, followed by
586 20 µl of M2-FLAG beads (Sigma). The mixture was rotated for 2 hours at 4˚C. M2-FLAG
587 beads were washed 4 times in TBS-T followed by 2 times in TBS. Finally, 35 µl of hot
588 (95˚C) SDS-PAGE Loading Buffer was added and the beads were heated for an
589 additional 5 minutes at 95˚C. Samples were electrophoresed on a gradient precast
590 SDS-PAGE gel (Biorad) and Coomassie stained. A lane of gel above the band with
591 unmodified Strep-IpaH2.5-3xFLAG-Ub or Strep-IpaH3-3xFLAG-Ub was excised, and
592 proteins were digested overnight with trypsin (Pierce) following reduction and alkylation
593 with DTT and iodoacetamide (Sigma–Aldrich). Following solid-phase extraction cleanup
594 with an Oasis HLB µelution plate (Waters), the resulting peptides were reconstituted in
595 10 µL of 2% (v/v) acetonitrile (ACN) and 0.1% trifluoroacetic acid in water. Two µL of

596 each sample were injected onto an Orbitrap Fusion Lumos (Thermo) mass
597 spectrometer, coupled to an Ultimate 3000 RSLC-Nano liquid chromatography systems
598 (Thermo) at the Mass Spectrometry Core at University of Texas Southwestern. Samples
599 were injected onto a 75 µm i.d., 75-cm long, (Lumos) EasySpray column (Thermo), and
600 eluted with a gradient from 0-28% buffer B over 90 minutes. Buffer A contained 2% (v/v)
601 ACN and 0.1% formic acid in water, and buffer B contained 80% (v/v) ACN, 10% (v/v)
602 trifluoroethanol, and 0.1% formic acid in water. The Orbitrap Fusion Lumos mass
603 spectrometer operated in positive ion mode with a source voltage of 2.0-2.4 kV and an
604 ion transfer tube temperature of 275 °C. MS scans were acquired at 120,000 resolution
605 in the Orbitrap and up to 10 MS/MS spectra were obtained in the Orbitrap for each full
606 spectrum acquired using higher-energy collisional dissociation (HCD) for ions with
607 charges 2-7. Dynamic exclusion was set for 25 seconds after an ion was selected for
608 fragmentation. Raw MS data files were analyzed using Proteome Discoverer v.2.4
609 (Thermo), with peptide identification performed using Sequest HT searching against the
610 human reviewed protein database from UniProt. Fragment and precursor tolerances of
611 10 ppm and 0.6 Da (Lumos) was specified, and three missed cleavages were allowed.
612 Carbamidomethylation of Cys was set as a fixed modification and oxidation of Met was
613 set as a variable modification. The false-discovery rate (FDR) cutoff was 1% for all
614 peptides. The abundance of identified peptides found for Strep-IpaH2.5 UBAIT were
615 compared to those found for control IpaH3 UBAIT that was included in the same
616 experiment. Hits for IpaH2.5 were included when abundance levels were at least 2-fold
617 higher than UBAIT controls.
618
619 **Statistical analysis**
620 Graphpad Prism 10.2.2 was used to generate graphs and to perform statistical
621 analyzes. Experiments were conducted in three to five biological replicates. Data in
622 graphs are displayed as mean ± standard error of the mean (SEM). Statistical analyses
623 included student t-test one-way and two-way analysis of variance (ANOVA) followed by
624 Tukey's multiple comparison tests. Significance was considered when p values were
625 <0.05
626

627 **Data storage**

628 A large UBAIT mass spectrometry dataset broadly probing for IpaH protein family
629 interaction partners was originally generated and published in (28). The numerical
630 values of all other quantified data depicted in data panels in this manuscript are openly
631 available in the Digital Repositories at Duke under the digital object identifier
632 doi.org/10.7924/r4vq36v59.

633

634 **ACKNOWLEDGEMENTS**

635 This work was supported by National Institutes of Health grants AI139425 (to JC),
636 AI083359 (to NMA), AI137031 (to NSH), and AI168107 (to NSH); and the Welch
637 Foundation (grant I-1704 to NMA). NSH holds an Investigators in the Pathogenesis of
638 Infectious Disease Award from the Burroughs Wellcome Fund. The funders had no role
639 in study design, data collection and interpretation, or the decision to submit the work for
640 publication. We would like to thank members of the Coers lab as well as the labs of Drs.
641 Clare Smith, David Tobin, and Edward Miao for providing valuable feedback.

642
643
644

645 **FIGURE LEGENDS**
646

647 **Fig. 1. Mutation of the bacterial transcription factor MxiE results in ubiquitylation**
648 **of *S. flexneri* in IFNγ-primed epithelial cells. (A - C)** Cells were primed with 100 U/ml
649 IFNγ or left unprimed and then infected with WT or *ΔmxiE S. flexneri* at an MOI of 50 -
650 100. Cells were fixed 3 - 4 h post infection (hpi) and stained for linear ubiquitin (M1-Ub)
651 with anti-M1 antibody. Percentage of M1-Ub-positive bacteria was quantified in infected
652 A549 epithelial cells at 4 hpi **(B)** and HT29 epithelial cells at 3 hpi **(C)**. Graphs show the
653 average of three independent experiments and depict means ± SEM. Two-way ANOVA
654 with Tukey's multiple comparison tests were performed; all statistically significant
655 comparisons are shown. ***p<0.001; **** p<0.0001; ns, not significant
656

657 **Fig. 2. *S. flexneri* Δ*mxiE* mutants become decorated with linear and lysine-linked**
658 **ubiquitin in IFNγ-primed A549 cells. (A)** WT A549 cells expressing the indicated
659 internally Strep-tagged Ubiquitin (INT-Ub) variants were primed with 100 U/ml IFNγ
660 overnight and co-localization of INT-Ub with cytosolic *S. flexneri* (Sf) Δ*mxiE* was
661 assessed at 4 hpi. Ubiquitin linkage-specific antibodies were used to determine the
662 percentage of *S. flexneri* Δ*mxiE* staining positive for K27-linked ubiquitin (K27-Ub) **(B)** or
663 K63-linked ubiquitin **(C)** in IFNγ-primed untransduced WT A549 cells. Co-staining of
664 anti-M1 and anti-ubiquitin (FK2) on the surface of *S. flexneri* Δ*mxiE* in IFNγ-primed
665 (100U/ml) A549 cells is shown in **(D)**. Quantification of anti-M1-FK2 co-staining in
666 untreated and IFNγ-primed A549 cells is depicted in **(E)**. All infections were done at an
667 MOI of 50 - 100. Data were generated from at least three independent experiments and
668 shows mean ± SEM. One-way ANOVA followed by Dunnet's multiple comparisons were
669 performed of all groups against WT-ubiquitin group **(A)**. Two-way ANOVA with Tukey's
670 multiple comparison tests were performed for **(B)** and **(C)**. An unpaired t-test was
671 performed between "both FK2+M1" groups (gray bars) (**E).** *p<0.05; **p<0.01;
672 ***p<0.001; **** p<0.0001
673

674 **Fig. 3 Ubiquitylation of *S.flexneri ΔmxiE* is dependent on RNF213 but not LUBAC**
675 **(A)** Immunoblotting for HOIP, HOIL-1, and RNF213 protein expression in untreated and

676 IFNγ-primed WT and the corresponding gene deletion (KO) A549 cells. **(B)** Percentage
677 Δ*mxiE S.flexneri* bacteria stained with anti-M1-linked ubiquitin in IFNγ-primed WT,
678 HOIP^{KO}, HOIL-1^{KO} and RNF213^{KO} A549 cells. **(C)** Percentage of WT and 7KR INT-Ub-
679 positive Δ*mxiE S. flexneri* in IFNγ-primed WT, HOIP^{KO}, and RNF213^{KO} A549 cells. **(D –**
680 **G)** Untreated and IFNγ-primed A549 and HT29 cells were infected with the indicated
681 *S. flexneri* strains and immuno-stained for RNF213 and ubiquitin (FK2). Representative
682 immunofluorescence microscopy images are shown for A549 infections in **(F).** RNF213-
683 *S. flexneri* colocalization percentages were quantified in A549 **(D)** and HT29 **(E)** cells.
684 **(G)** Quantification of ubiquitin and RNF213 colocalization with Δ*mxiE S. flexneri* in A549
685 cells. Percentages of Δ*mxiE S. flexneri* staining positive for antibodies specific for K27-
686 linked **(H)** and K63-linked ubiquitin **(I)** are also provided. All data are represented by the
687 mean ± SEM from at least three independent experiments. One-way ANOVA followed
688 by Dunnet's multiple comparisons were performed of all groups against WT A549 group
689 in **(A)**. Two-way ANOVA with Tukey's multiple comparison tests were performed in **(C, D**
690 and **F)**. an unpaired t-test was performed between the "Ub+ & RNF213+" groups (gray
691 bars) in **(G)**. For **(H** and **I)**, an unpaired-t test was performed. Comparisons not shown
692 are non-significant. **p<0.01;; **** p<0.0001
693
694 **Fig. 4. *S. flexneri* virulence factors IpaH1.4 and IpaH2.5 induce proteasomal**
695 **degradation of RNF213 (A-B)** All *S. flexneri* strains express PilT to enhance adhesion
696 and infection rates and infections were carried out at an MOI of 5 - 25 for 3 hours **(A)**
697 Untreated and IFNγ-primed (100 U/ml) A549 cells were infected with indicated *S.*
698 *flexneri* strains expressing GFP. Protein lysates were probed for expression of RNF213,
699 HOIP, and GFP. GFP expression serves as a bacterial protein loading control. **(B)**
700 Infected and uninfected A549 cells were cultured in the presence of different
701 concentrations of the proteasomal inhibitor MG132 and RNF213 expression was
702 monitored by immunoblotting. **(C)** HEK 293T cells stably expressing mCherry-RNF213
703 were transiently transfected with individual GFP-tagged IpaH effectors for 24 hours and
704 RNF213 expression was assessed. **(D)** WT and catalytically inactive C368S mutants of
705 IpaH1.4 and IpaH2.5 were transiently transfected into HEK 293T cells expressing
706 mCherry-RNF213 and cell lysates were subjected to immunoblotting. **(C-D)**

707 Denaturation of cell lysates at lower temperature (56°C) was required for RNF213
708 detection but also resulted in the formation of double bands for all IpaH-GFP constructs.
709 Images are representative of three independent experiments UI: Uninfected.
710
711 **Fig. 5. Loss of IpaH1.4 is sufficient to render *S. flexneri* susceptible to RNF213-**
712 **driven ubiquitylation (A)** IFNγ-primed WT and HOIP^{KO} A549 cells were infected with
713 the indicated PilT^{+}, GFP^{+} *S. flexneri* strains for 3 hours at an MOI of 25 and RNF213
714 protein levels were assessed by Western blotting. Bacterial GFP and host actin are
715 used as host protein loading controls. **(B)** Percentages of RNF213^{+} WT and Δ*ipaH1.4*
716 *S. flexneri* in IFNγ-primed A549 cells are shown. **(C)** Representative microscopy images
717 depicting RNF213 recruitment to cytosolic Δ*IpaH1.4* bacteria complemented with empty
718 vector, WT IpaH1.4, or catalytically inactive IpaH1.4 (C368S) in IFNγ-primed WT A549
719 cells. **(D)** Percentages of RNF213^{+} indicated *S. flexneri* strains in IFNγ-primed WT A549
720 cells are shown. **(E)** Percentages WT and Δ*IpaH1.4 S. flexneri* stained positive for anti-
721 M1-linked antibody in IFNγ-primed WT and RNF213^{KO} A549 cells are depicted. **(F)** The
722 ilux operon was introduced into *S. flexneri* strains to use bioluminescence relative light
723 units (RLU) as a proxy for bacterial growth. RLU was measured in IFNγ-primed WT
724 A549 cells infected with the indicated *S. flexneri* strains at an MOI of 5. **(B, D, E)** Data
725 represent the mean ± SEM from at least three independent experiments. An unpaired t-
726 test was conducted for **(B)**. One-way ANOVA followed by Dunnet's multiple
727 comparisons were performed between all groups against the group Δ*ipaH1.4*
728 expressing WT IpaH1.4 **(D)** and WT A549 cells **(E).** *p<0.05; ***p<0.001; **** p<0.0001
729
730

REFERENCES

1. J. L. Casanova, J. D. MacMicking, C. F. Nathan, Interferon-gamma and infectious diseases: Lessons and prospects. *Science* **384**, eadl2016 (2024).
2. D. Hernandez, S. Walsh, L. Saavedra Sanchez, M. S. Dickinson, J. Coers, Interferon-Inducible E3 Ligase RNF213 Facilitates Host-Protective Linear and K63-Linked Ubiquitylation of Toxoplasma gondii Parasitophorous Vacuoles. *mBio* 10.1128/mbio.01888-22, e0188822 (2022).
3. E. G. Otten *et al.*, Ubiquitylation of lipopolysaccharide by RNF213 during bacterial infection. *Nature* **594**, 111-116 (2021).
4. S. C. Walsh *et al.*, The bacterial effector GarD shields Chlamydia trachomatis inclusions from RNF213-mediated ubiquitylation and destruction. *Cell Host Microbe* 10.1016/j.chom.2022.08.008 (2022).
5. D. Houzelstein *et al.*, The ring finger protein 213 gene (Rnf213) contributes to Rift Valley fever resistance in mice. *Mamm Genome* **32**, 30-37 (2021).
6. F. Thery *et al.*, Ring finger protein 213 assembles into a sensor for ISGylated proteins with antimicrobial activity. *Nat Commun* **12**, 5772 (2021).
7. S. K. Matta *et al.*, Genome-wide and targeted CRISPR screens identify RNF213 as a mediator of interferon gamma-dependent pathogen restriction in human cells. *Proc Natl Acad Sci U S A* **121**, e2315865120 (2024).
8. L. Martina *et al.*, Proteome Profiling of RNF213 Depleted Cells Reveals Nitric Oxide Regulator DDAH1 Antilisterial Activity. *Frontiers in cellular and infection microbiology* **11**, 735416 (2021).
9. J. Noad *et al.*, LUBAC-synthesized linear ubiquitin chains restrict cytosol-invading bacteria by activating autophagy and NF-kappaB. *Nat Microbiol* **2**, 17063 (2017).
10. M. Szczesna *et al.*, Bacterial esterases reverse lipopolysaccharide ubiquitylation to block host immunity. *Cell Host Microbe* **32**, 913-924 e917 (2024).
11. C. Troeger *et al.*, Global disability-adjusted life-year estimates of long-term health burden and undernutrition attributable to diarrhoeal diseases in children younger than 5 years. *Lancet Glob Health* **6**, e255-e269 (2018).
12. T. E. Libby *et al.*, Consequences of Shigella infection in young children: a systematic review. *Int J Infect Dis* **129**, 78-95 (2023).
13. K. H. Bagamian, J. D. Anderson Iv, G. Blohm, S. Scheele, Shigella and childhood stunting: Evidence, gaps, and future research directions. *PLoS Negl Trop Dis* **17**, e0011475 (2023).
14. N. Mellouk, J. Enninga, Cytosolic Access of Intracellular Bacterial Pathogens: The Shigella Paradigm. *Frontiers in cellular and infection microbiology* **6**, 35 (2016).
15. M. M. Levine, K. L. Kotloff, E. M. Barry, M. F. Pasetti, M. B. Sztein, Clinical trials of Shigella vaccines: two steps forward and one step back on a long, hard road. *Nat Rev Microbiol* **5**, 540-553 (2007).
16. R. Raqib *et al.*, Persistence of local cytokine production in shigellosis in acute and convalescent stages. *Infect Immun* **63**, 289-296 (1995).
17. R. Raqib, B. Wretlind, J. Andersson, A. A. Lindberg, Cytokine secretion in acute shigellosis is correlated to disease activity and directed more to stool than to plasma. *J Infect Dis* **171**, 376-384 (1995).

775 18. M. Kutsch, C. Gonzalez-Prieto, J. Coers, The GBP1 microcapsule interferes with IcsA-
776 dependent septin cage assembly around Shigella flexneri. *Pathog Dis* **79** (2021).
777 19. M. Kutsch *et al.*, Direct binding of polymeric GBP1 to LPS disrupts bacterial cell envelope
778 functions. *EMBO J* **39**, e104926 (2020).
779 20. A. S. Piro *et al.*, Detection of Cytosolic Shigella flexneri via a C-Terminal Triple-Arginine
780 Motif of GBP1 Inhibits Actin-Based Motility. *mBio* **8** (2017).
781 21. M. P. Wandel *et al.*, GBPs Inhibit Motility of Shigella flexneri but Are Targeted for
782 Degradation by the Bacterial Ubiquitin Ligase IpaH9.8. *Cell Host Microbe* **22**, 507-518
783 e505 (2017).
784 22. L. Goers *et al.*, Shigella IpaH9.8 limits GBP1-dependent LPS release from intracytosolic
785 bacteria to suppress caspase-4 activation. *Proc Natl Acad Sci U S A* **120**, e2218469120
786 (2023).
787 23. P. Li *et al.*, Ubiquitination and degradation of GBPs by a Shigella effector to suppress host
788 defence. *Nature* (2017).
789 24. A. Bullones-Bolanos, J. Bernal-Bayard, F. Ramos-Morales, The NEL Family of Bacterial E3
790 Ubiquitin Ligases. *Int J Mol Sci* **23** (2022).
791 25. P. Schnupf, P. J. Sansonetti, Shigella Pathogenesis: New Insights through Advanced
792 Methodologies. *Microbiol Spectr* **7** (2019).
793 26. C. D. Kane, R. Schuch, W. A. Day, Jr., A. T. Maurelli, MxiE regulates intracellular expression
794 of factors secreted by the Shigella flexneri 2a type III secretion system. *J Bacteriol* **184**,
795 4409-4419 (2002).
796 27. M. Mavris, P. J. Sansonetti, C. Parsot, Identification of the cis-acting site involved in
797 activation of promoters regulated by activity of the type III secretion apparatus in
798 Shigella flexneri. *J Bacteriol* **184**, 6751-6759 (2002).
799 28. M. F. de Jong, Z. Liu, D. Chen, N. M. Alto, Shigella flexneri suppresses NF-kappaB
800 activation by inhibiting linear ubiquitin chain ligation. *Nat Microbiol* **1**, 16084 (2016).
801 29. J. Liu *et al.*, Mechanistic insights into the subversion of the linear ubiquitin chain
802 assembly complex by the E3 ligase IpaH1.4 of Shigella flexneri. *Proc Natl Acad Sci U S A*
803 **119**, e2116776119 (2022).
804 30. K. Hiragi *et al.*, Structural insight into the recognition of the linear ubiquitin assembly
805 complex by Shigella E3 ligase IpaH1.4/2.5. *J Biochem* **173**, 317-326 (2023).
806 31. G. Luchetti *et al.*, Shigella ubiquitin ligase IpaH7.8 targets gasdermin D for degradation to
807 prevent pyroptosis and enable infection. *Cell Host Microbe* **29**, 1521-1530 e1510 (2021).
808 32. J. M. Hansen *et al.*, Pathogenic ubiquitination of GSDMB inhibits NK cell bactericidal
809 functions. *Cell* **184**, 3178-3191 e3118 (2021).
810 33. R. Otsubo *et al.*, Shigella effector IpaH4.5 targets 19S regulatory particle subunit RPN13
811 in the 26S proteasome to dampen cytotoxic T lymphocyte activation. *Cell Microbiol* **21**,
812 e12974 (2019).
813 34. J. R. Rohde, A. Breitkreutz, A. Chenal, P. J. Sansonetti, C. Parsot, Type III secretion
814 effectors of the IpaH family are E3 ubiquitin ligases. *Cell Host Microbe* **1**, 77-83 (2007).
815 35. H. Ashida *et al.*, A bacterial E3 ubiquitin ligase IpaH9.8 targets NEMO/IKKgamma to
816 dampen the host NF-kappaB-mediated inflammatory response. *Nat Cell Biol* **12**, 66-73;
817 sup pp 61-69 (2010).

36. K. Naydenova *et al.*, Shigella flexneri evades LPS ubiquitylation through IpaH1.4-mediated degradation of RNF213. *Nat Struct Mol Biol* 10.1038/s41594-025-01530-8 (2025).
37. X. Zhou *et al.*, Shigella effector IpaH1.4 subverts host E3 ligase RNF213 to evade antibacterial immunity. *Nat Commun* **16**, 3099 (2025).
38. N. Silue, E. Marcantonio, F. X. Campbell-Valois, RNA-Seq analysis of the T3SA regulon in Shigella flexneri reveals two new chromosomal genes upregulated in the on-state. *Methods* **176**, 71-81 (2020).
39. C. Ji *et al.*, Structural mechanism for guanylate-binding proteins (GBPs) targeting by the Shigella E3 ligase IpaH9.8. *PLoS Pathog* **15**, e1007876 (2019).
40. I. Tripathi-Giesgen, C. Behrends, A. F. Alpi, The ubiquitin ligation machinery in the defense against bacterial pathogens. *EMBO Rep* **22**, e52864 (2021).
41. A. K. Haldar *et al.*, Ubiquitin systems mark pathogen-containing vacuoles as targets for host defense by guanylate binding proteins. *Proc Natl Acad Sci U S A* **112**, E5628-5637 (2015).
42. M. C. Fernandez *et al.*, CT135 mediates the resistance of Chlamydia trachomatis to primate interferon gamma stimulated immune defenses. *iScience* **27**, 110143 (2024).
43. D. Komander, M. Rape, The ubiquitin code. *Annual review of biochemistry* **81**, 203-229 (2012).
44. I. Dikic, B. A. Schulman, An expanded lexicon for the ubiquitin code. *Nature reviews. Molecular cell biology* **24**, 273-287 (2023).
45. T. Kirisako *et al.*, A ubiquitin ligase complex assembles linear polyubiquitin chains. *EMBO J* **25**, 4877-4887 (2006).
46. K. Sasaki, K. Iwai, LUBAC-mediated linear ubiquitination in tissue homeostasis and disease. *J Biochem* **174**, 99-107 (2023).
47. L. Gao *et al.*, The mechanism of linear ubiquitination in regulating cell death and correlative diseases. *Cell death & disease* **14**, 659 (2023).
48. N. Alphonse *et al.*, A family of conserved bacterial virulence factors dampens interferon responses by blocking calcium signaling. *Cell* **185**, 2354-2369 e2317 (2022).
49. D. Ruano-Gallego *et al.*, Type III secretion system effectors form robust and flexible intracellular virulence networks. *Science* **371** (2021).
50. J. Sanchez-Garrido, D. Ruano-Gallego, J. S. Choudhary, G. Frankel, The type III secretion system effector network hypothesis. *Trends Microbiol* **30**, 524-533 (2022).
51. C. S. Tsai *et al.*, Shigellosis in Taiwan: An old enteric pathogen with changing epidemiology and increasing antimicrobial resistance. *J Microbiol Immunol Infect* **57**, 346-353 (2024).
52. E. S. Donkor, A. Odoom, A. H. Osman, S. Darkwah, F. C. N. Kotey, A Systematic Review on Antimicrobial Resistance in Ghana from a One Health Perspective. *Antibiotics (Basel)* **13** (2024).
53. X. M. Matanza, A. Clements, Pathogenicity and virulence of Shigella sonnei: A highly drug-resistant pathogen of increasing prevalence. *Virulence* **14**, 2280838 (2023).
54. H. O'Flanagan, M. Siddiq, C. Llewellyn, D. Richardson, Antimicrobial resistance in sexually transmitted Shigella in men who have sex with men: A systematic review. *Int J STD AIDS* **34**, 374-384 (2023).

862 55. J. Coers *et al.*, Chlamydia muridarum evades growth restriction by the IFN-gamma-
863 inducible host resistance factor Irgb10. *J Immunol* **180**, 6237-6245 (2008).
864 56. M. Sugihara *et al.*, The AAA+ ATPase/ubiquitin ligase mysterin stabilizes cytoplasmic lipid
865 droplets. *J Cell Biol* **218**, 949-960 (2019).
866 57. S. I. Kim *et al.*, Inducible Transgene Expression in Human iPS Cells Using Versatile All-in-
867 One piggyBac Transposons. *Methods Mol Biol* **1357**, 111-131 (2016).
868 58. S. Skavicus, N. S. Heaton, Approaches for timeline reductions in pathogenesis studies
869 using genetically modified mice. *Microbiol Spectr* **11**, e0252123 (2023).
870 59. C. B. Gurumurthy *et al.*, Creation of CRISPR-based germline-genome-engineered mice
871 without ex vivo handling of zygotes by i-GONAD. *Nature protocols* **14**, 2452-2482 (2019).
872 60. M. Ohtsuka *et al.*, i-GONAD: a robust method for in situ germline genome engineering
873 using CRISPR nucleases. *Genome Biol* **19**, 25 (2018).
874 61. B. P. Cormack, R. H. Valdivia, S. Falkow, FACS-optimized mutants of the green fluorescent
875 protein (GFP). *Gene* **173**, 33-38 (1996).
876 62. M. Valenzuela-Ortega, C. French, Joint universal modular plasmids (JUMP): a flexible
877 vector platform for synthetic biology. *Synth Biol (Oxf)* **6**, ysab003 (2021).
878 63. C. Gregor, K. C. Gwosch, S. J. Sahl, S. W. Hell, Strongly enhanced bacterial
879 bioluminescence with the ilux operon for single-cell imaging. *Proc Natl Acad Sci U S A*
880 **115**, 962-967 (2018).
881 64. M. S. Dickinson *et al.*, LPS-aggregating proteins GBP1 and GBP2 are each sufficient to
882 enhance caspase-4 activation both in cellulo and in vitro. *Proc Natl Acad Sci U S A* **120**,
883 e2216028120 (2023).
884 65. P. Clerc, P. J. Sansonetti, Entry of Shigella flexneri into HeLa cells: evidence for directed
885 phagocytosis involving actin polymerization and myosin accumulation. *Infect Immun* **55**,
886 2681-2688. (1987).
887
888

889 **SUPPLEMENTARY FIGURE LEGENDS**
890

891 **Fig. S1 Addition of an N-terminal HA-tag significantly reduces targeting of 7KR**
892 **ubiquitin to *S. flexneri* Δ*mxiE*.** N-terminally untagged and N-terminally HA-tagged
893 versions of the internally Strep-tagged Ubiquitin (INT-Ub) 7KR mutant variant were
894 expressed in A549 cells. Cells were primed with 100 U/ml IFNγ overnight and co-
895 localization of INT-Ub with cytosolic *S. flexneri* (Sf) Δ*mxiE* was assessed at 4 hpi. An
896 unpaired t-test was conducted. **p<0.01
897

898 **Fig. S2 Ubiquitin-Activated Interaction Trap (UBAIT) identifies mouse Rnf213 as**
899 **likely interaction partner of IpaH2.5. (A)** Diagram showing the experimental
900 procedure for UBAIT detection of IpaH2.5 and IpaH3 (control) substrates from the colon
901 and caecum of mice infected with *Salmonella enterica* Typhimurium (S. Tm). **(B)** Mass
902 spectrometry of hits identified in the Strep-IpaH2.5 UBAIT (left) as compared to Strep-
903 IpaH3 UBAIT (right). The top 12 proteins identified in the Strep-IpaH2.5 UBAIT samples
904 as determined by peptide abundance are shown. The corresponding peptide
905 abundances from Strep-IpaH3 UBAIT are shown. RNF213 and the previously identified
906 IpaH2.5 substrate RNF31 (HOIP) are highlighted. PSM = peptide spectrum match. ND
907 = Not Detected. NR = Not Reported.
908

909 **Fig. S3 Deletion of *ipaH1.4* but not *ipaH2.5* results in RNF213 recruitment to**
910 **cytosolic *S. flexneri*. (A)** A549 cells were primed with IFNγ (100 U/ml) and infected
911 with the indicated strains expressing GFP for 4 hours at an MOI of 100. RNF213
912 recruitment to cytosolic bacteria was quantified. **(B)** IFNγ-primed A549 RNF213^{KO} cells
913 were infected with the indicated PilT^{+} *S. flexneri* strains for 3 hours at an MOI of 25 and
914 HOIP protein levels were assessed by Western blotting. **(C)** Representative microscopy
915 images showing anti-M1-linked ubiquitin staining of Δ*ipaH1.4 S. flexneri* bacteria in
916 IFNγ-primed WT A549 cells. Quantified data are shown in Fig. 5E. Percentages of WT
917 and Δ*ipaH1.4 S. flexneri* bacteria stained with anti-K27-linked ubiquitin **(D)** or anti-K63-
918 linked ubiquitin **(E)** in IFNγ-primed WT A549 cells. **(F)** Percentages of anti-M1-linked
919 ubiquitin positive Δ*ipaH1.4 S. flexneri* bacteria in IFNγ-primed WT, RNF213^{KO}, HOIL-1^{KO}

920 and HOIP^{KO} A549 cells. Data are represented by the mean ± SEM from three
921 independent experiments. An unpaired t-test was conducted for **(D, E)**. Data are
922 represented by the mean ± SEM from three independent experiments. Two-way ANOVA
923 with Tukey's multiple comparison tests were performed for **(A,F)**; all statistically
924 significant comparisons are shown. **** p<0.0001; ***p<0.001; **p<0.01; ns, not
925 significant
926
927 **Fig. S4 Mouse Rnf213 binds to Δ*ipaH1.4 S. flexneri* and facilitates linear**
928 **ubiquitylation of cytosolic bacteria**
929 **(A)** Immunoblotting for mouse Rnf213 protein expression in untreated and IFNγ-primed
930 WT and IFNγ-primed Rnf213^{KO} MEF cells. Each lane represents MEFs from separate
931 mouse embryos that were used for infections. **(B and C)** MEF cells were primed with
932 mouse IFNγ (100 U/ml) and infected with the indicated strains expressing GFP and PilT
933 for 2 hours at an MOI of 100. Rnf213-*S. flexneri* colocalization percentages were
934 quantified and are shown in **(B)**. **(C)** Percentage of M1-linked ubiquitin positive *S.*
935 *flexneri* in IFNγ-primed WT and Rnf213^{KO} MEF cells. All data are represented by the
936 mean ± SEM from at least three independent experiments. An unpaired t-test was
937 performed in **(B)**. Two-way ANOVA with Tukey's multiple comparison tests were
938 performed in **(C)**. **p<0.01; **** p<0.0001
939

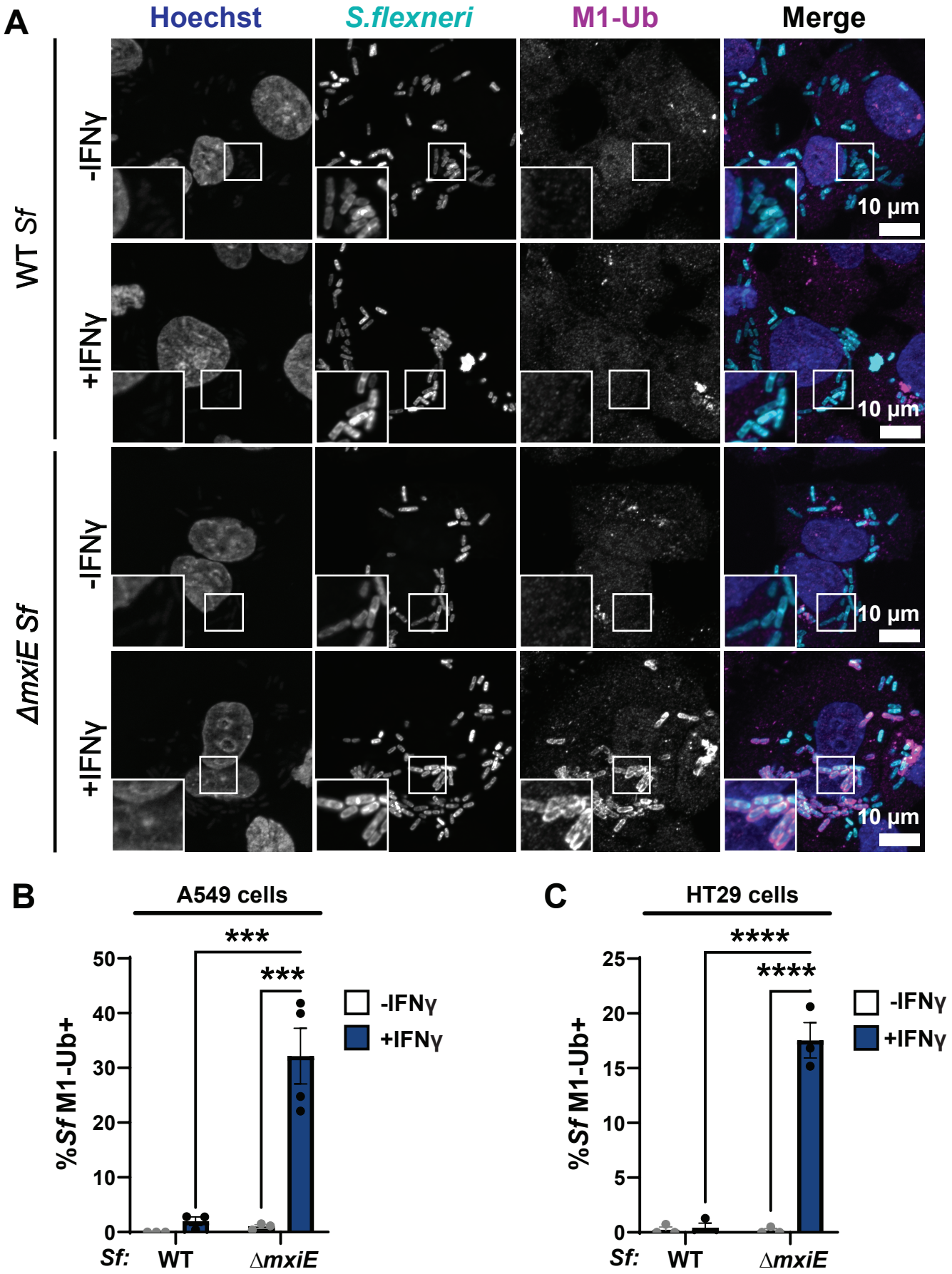
A
Hoechst
S.flexneri
M1-Ub
Merge
WT Sf
ΔmxiE Sf
-IFNγ
+IFNγ
10 µm
B
A549 cells
%Sf M1-Ub+
***
***
-IFNγ
+IFNγ
Sf:
WT
ΔmxiE
C
HT29 cells
%Sf M1-Ub+
****
****
-IFNγ
+IFNγ
Sf:
WT
ΔmxiE

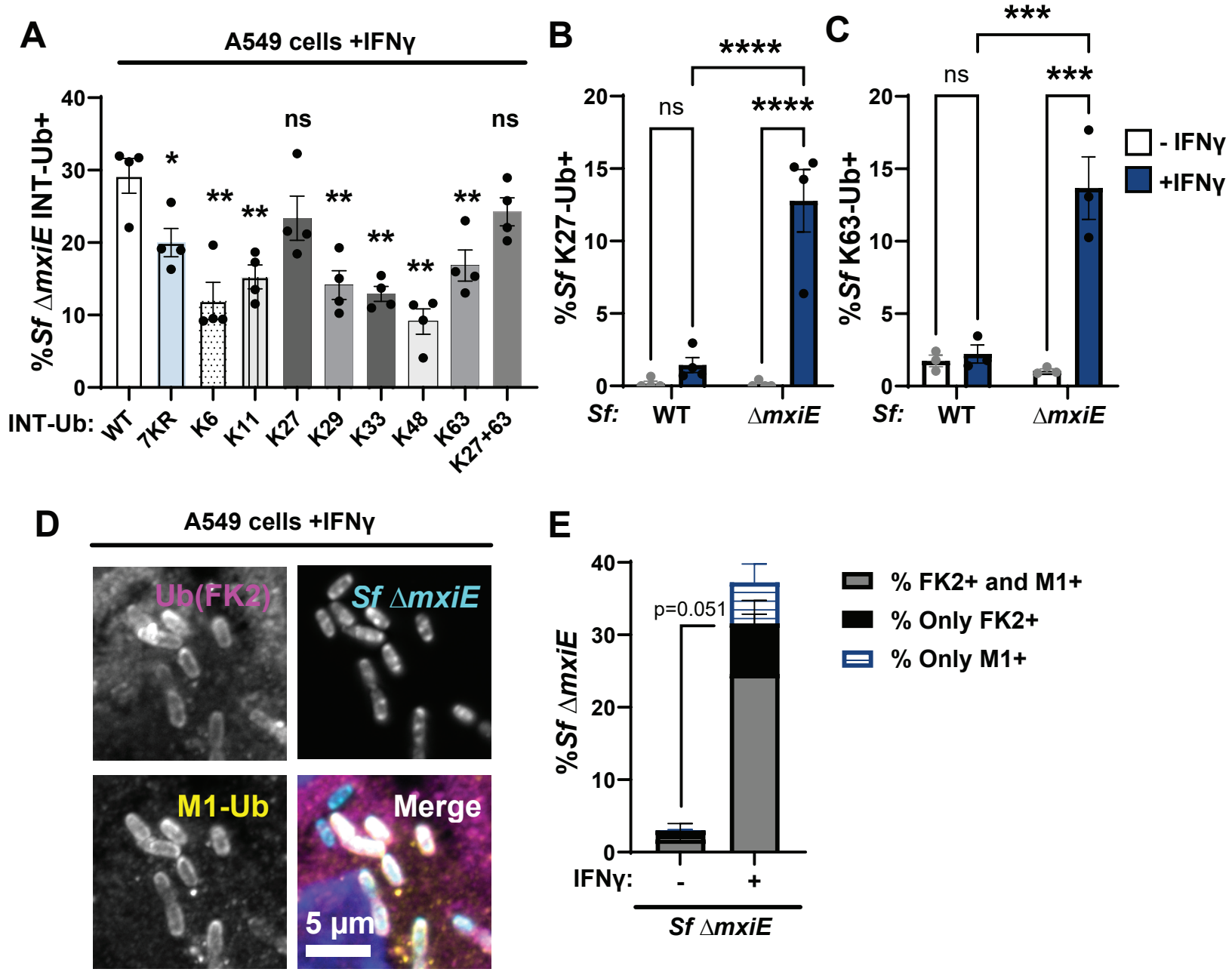
A
A549 cells +IFNγ
%Sf ΔmxiE INT-Ub+
INT-Ub:
WT
7KR
K6
K11
K27
K29
K33
K48
K63
K27+63
ns
B
%Sf K27-Ub+
Sf:
WT
ΔmxiE
C
%Sf K63-Ub+
- IFNγ
+IFNγ
D
A549 cells +IFNγ
Ub(FK2)
Sf ΔmxiE
M1-Ub
Merge
5 µm
E
%Sf ΔmxiE
p=0.051
IFNγ:
% FK2+ and M1+
% Only FK2+
% Only M1+

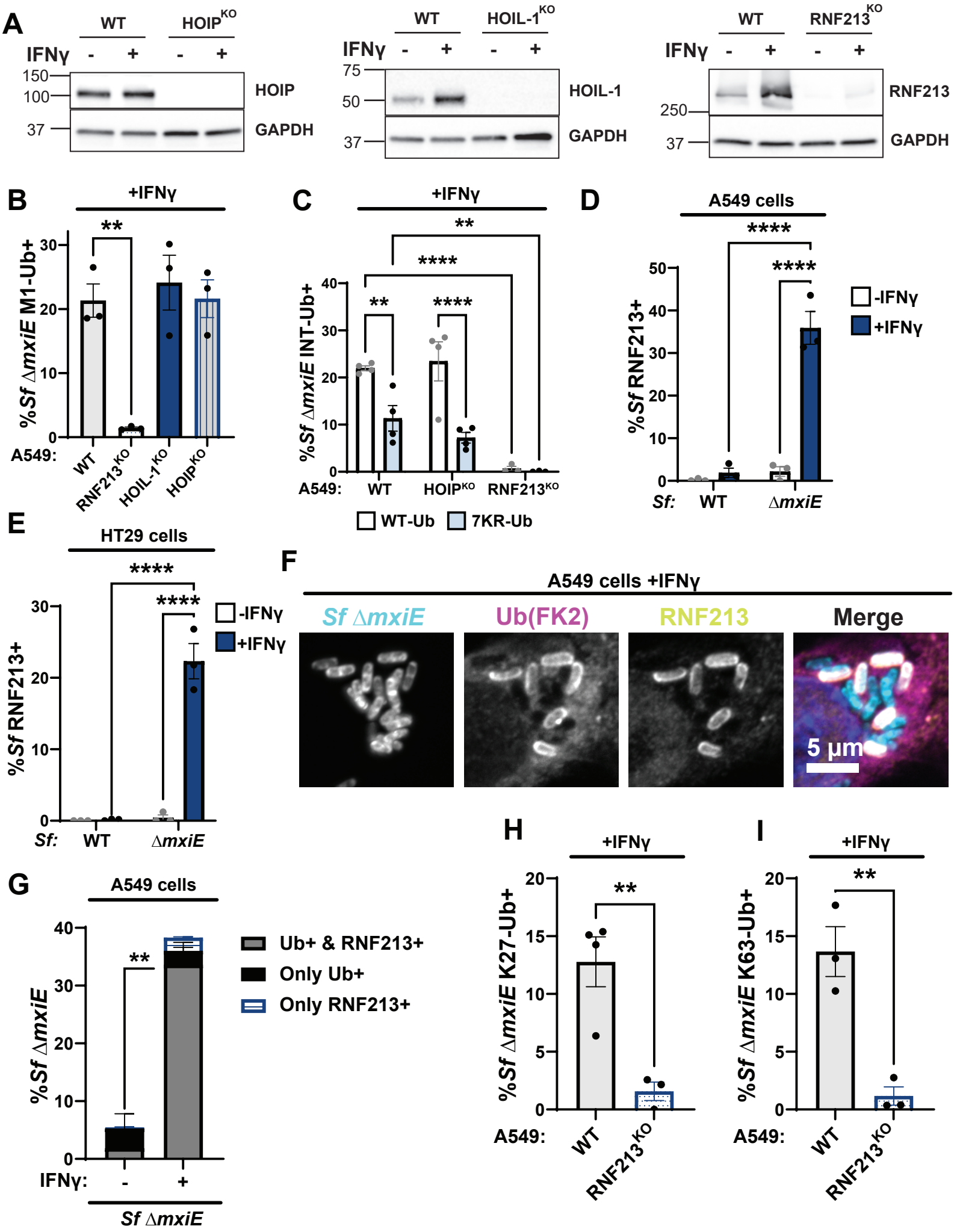
A
WT
HOIP^KO
IFNγ - + - +
150
100
37
HOIP
GAPDH
WT
HOIL-1^KO
IFNγ - + - +
75
50
37
HOIL-1
GAPDH
WT
RNF213^KO
IFNγ - + - +
250
37
RNF213
GAPDH
B
+IFNγ
**
%Sf ΔmxiE M1-Ub+
A549:
WT
RNF213^KO
HOIL-1^KO
HOIP^KO
C
+IFNγ
**
****
**
****
%Sf ΔmxiE INT-Ub+
A549:
WT
HOIP^KO
RNF213^KO
WT-Ub
7KR-Ub
D
A549 cells
****
****
%Sf RNF213+
-IFNγ
+IFNγ
Sf:
WT
ΔmxiE
E
HT29 cells
****
****
%Sf RNF213+
-IFNγ
+IFNγ
Sf:
WT
ΔmxiE
F
A549 cells +IFNγ
Sf ΔmxiE
Ub(FK2)
RNF213
Merge
5 µm
G
A549 cells
**
%Sf ΔmxiE
Ub+ & RNF213+
Only Ub+
Only RNF213+
IFNγ:
-
+
Sf ΔmxiE
H
+IFNγ
**
%Sf ΔmxiE K27-Ub+
A549:
WT
RNF213^KO
I
+IFNγ
**
%Sf ΔmxiE K63-Ub+
A549:
WT
RNF213^KO

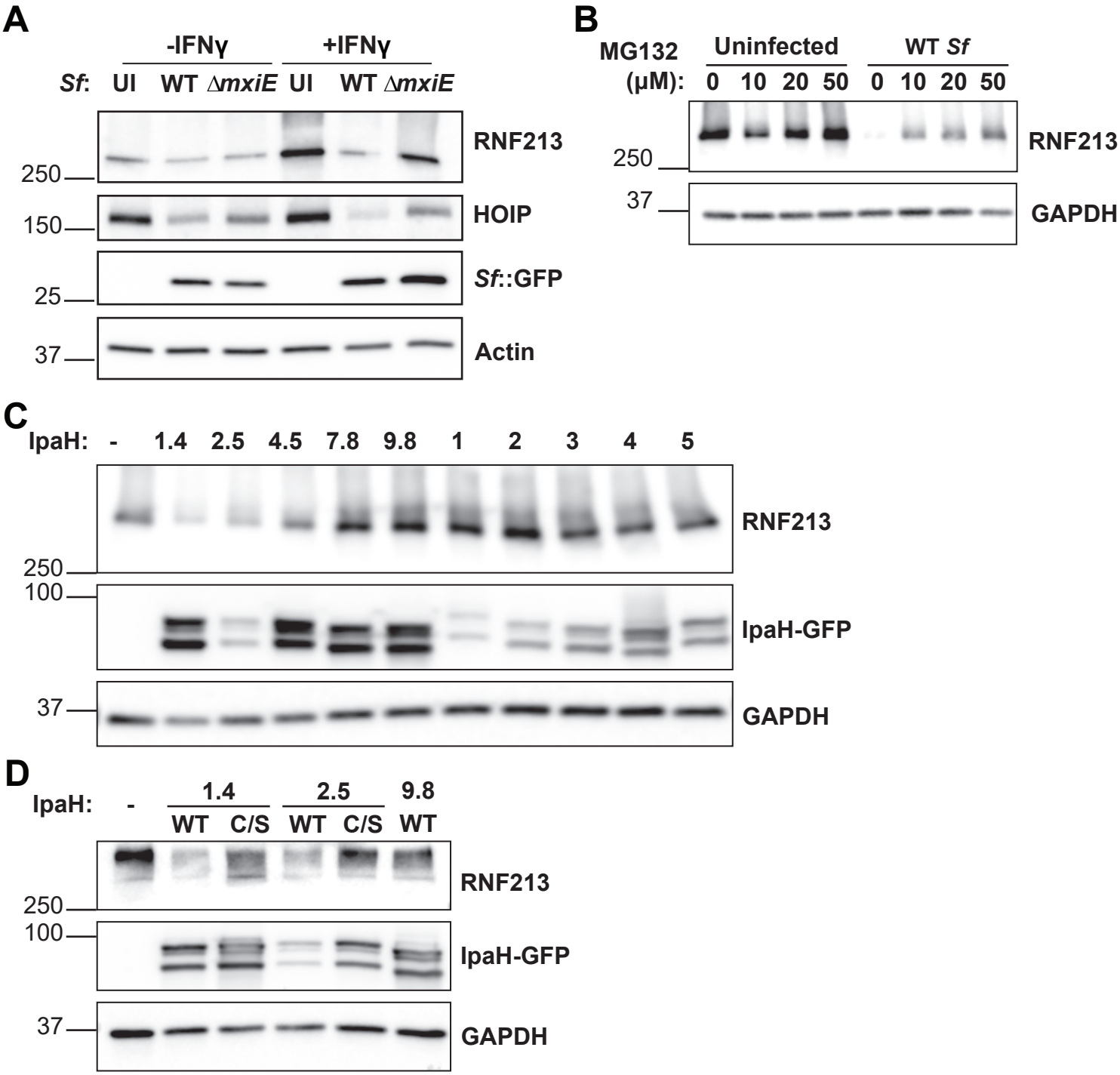
A
-IFNγ
+IFNγ
Sf: UI WT ΔmxiE UI WT ΔmxiE
250
150
25
37
RNF213
HOIP
Sf::GFP
Actin
B
MG132 (μM): Uninfected 0 10 20 50
WT Sf 0 10 20 50
250
37
RNF213
GAPDH
C
IpaH: - 1.4 2.5 4.5 7.8 9.8 1 2 3 4 5
250
100
37
RNF213
IpaH-GFP
GAPDH
D
IpaH: - 1.4 WT C/S 2.5 WT C/S 9.8 WT
250
100
37
RNF213
IpaH-GFP
GAPDH

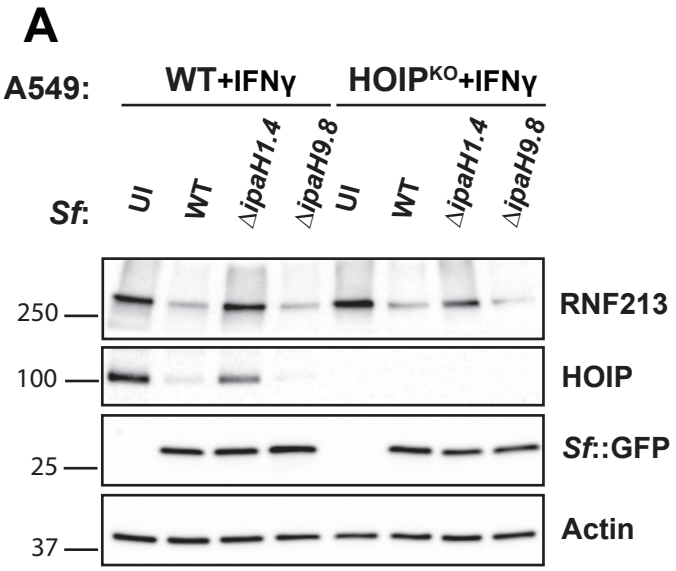
A
A549:
WT+IFNγ
HOIP^KO+IFNγ
Sf:
UI
WT
ΔipaH1.4
ΔipaH9.8
UI
WT
ΔipaH1.4
ΔipaH9.8
250
100
25
37
RNF213
HOIP
Sf::GFP
Actin

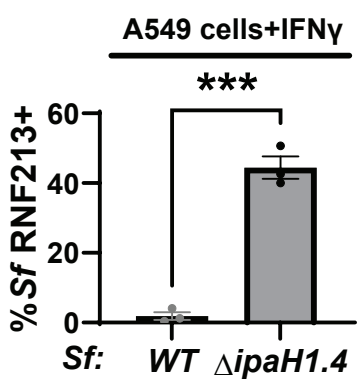
B
A549 cells+IFNγ
***
% Sf RNF213+
60
40
20
0
Sf:
WT
ΔipaH1.4

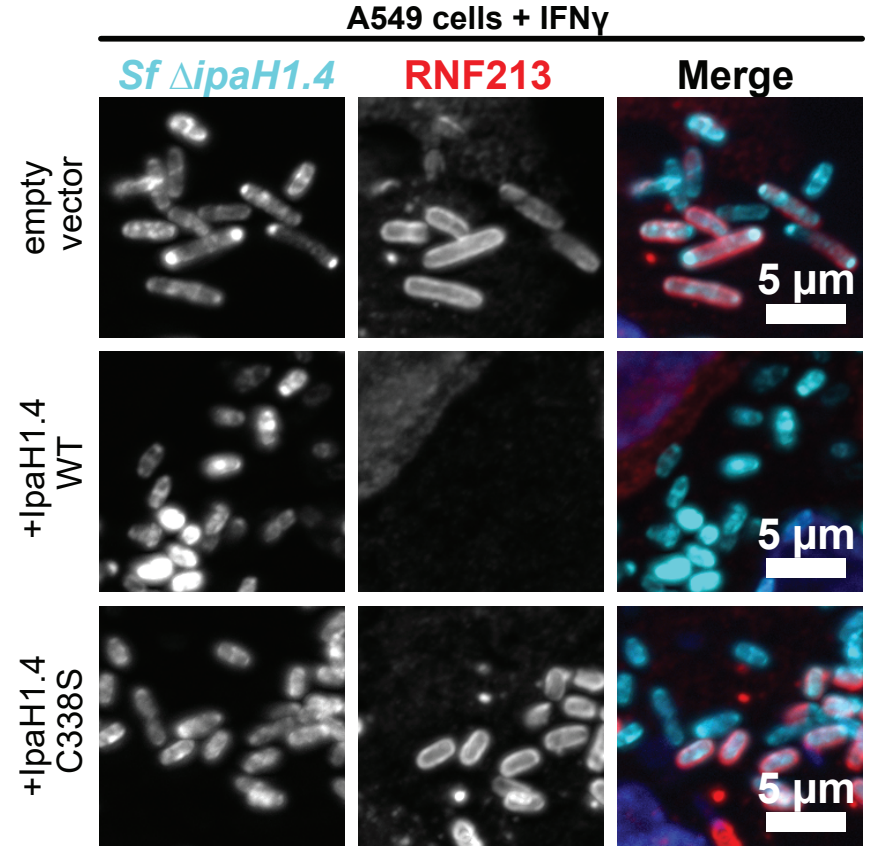
C
A549 cells + IFNγ
Sf ΔipaH1.4
RNF213
Merge
empty vector
+IpaH1.4 WT
+IpaH1.4 C338S
5 µm
5 µm
5 µm

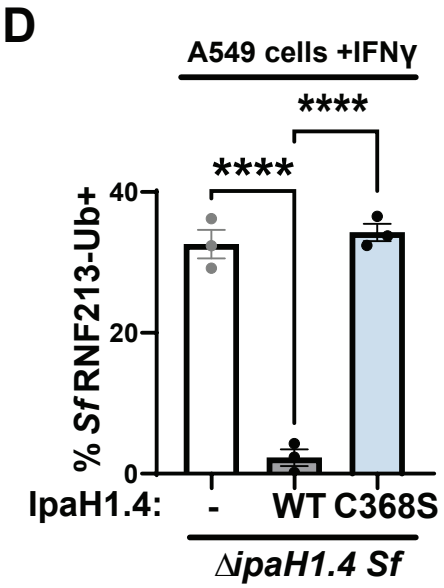
D
A549 cells +IFNγ
****
****
% Sf RNF213-Ub+
40
20
0
IpaH1.4:
-
WT
C368S
ΔipaH1.4 Sf

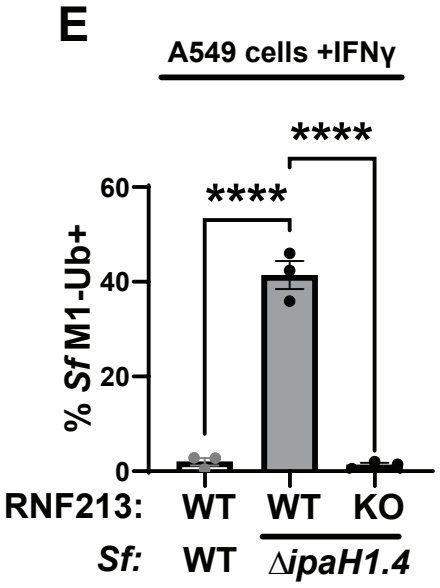
E
A549 cells +IFNγ
****
****
% Sf M1-Ub+
60
40
20
0
RNF213:
WT
WT
KO
Sf:
WT
ΔipaH1.4

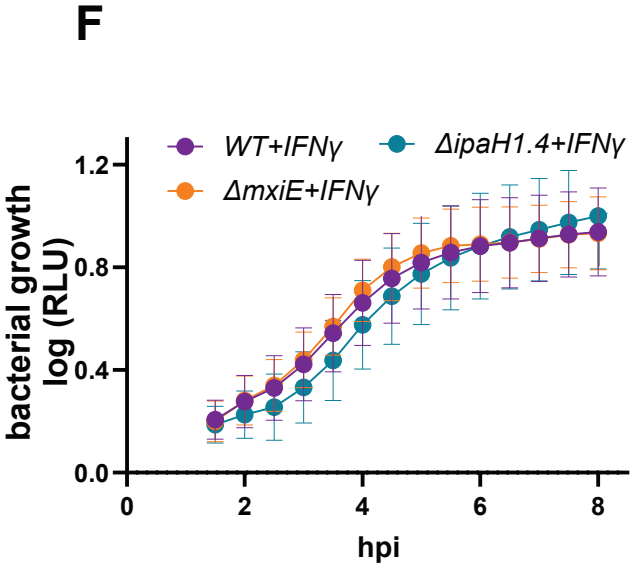
F
WT+IFNγ
ΔipaH1.4+IFNγ
ΔmxiE+IFNγ
bacterial growth log (RLU)
1.2
0.8
0.4
0.0
0
2
4
6
8
hpi

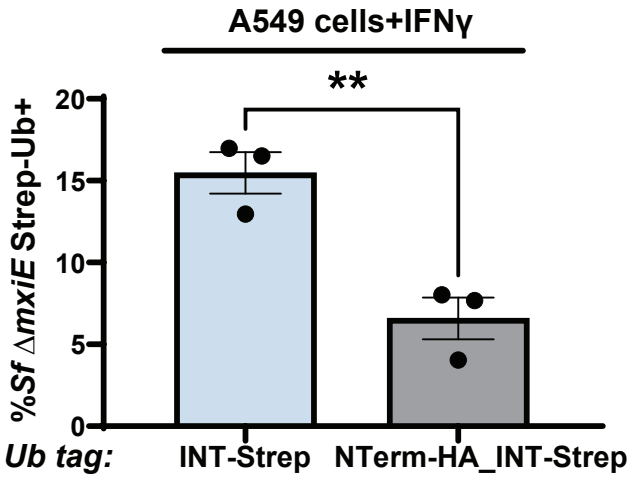
A549 cells+IFNγ
**
%Sf ΔmxiE Strep-Ub+
20
15
10
5
0
Ub tag:
INT-Strep
NTerm-HA_INT-Strep

A

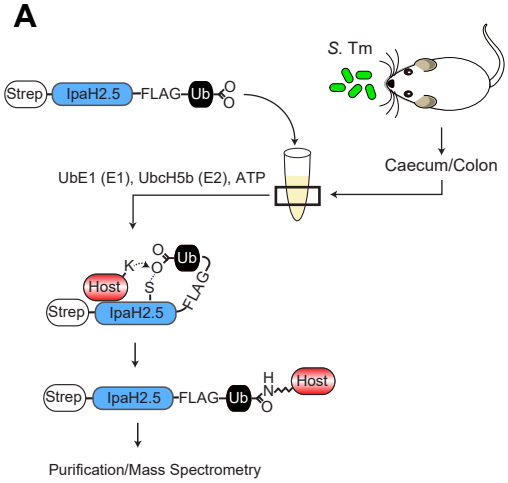

B

			Strep-IpaH2.5 UBAIT				Strep-IpaH3 UBAIT			
Gene	Accession	Molecular Weight	Abundance	Number of Peptides	Number of PSMs	Percent Coverage	Abundance	Number of Peptides	Number of PSMs	Percent Coverage
Rnf213	**E9Q555**	**584.3**	**3.51E+07**	**157**	**174**	**37**	**8.33E+04**	**4**	**4**	**1**
Ubr4	A2AN08	571.9	2.14E+06	29	29	9	4.56E+04	4	4	1
Rnf31	Q924T7	119.2	4.33E+06	28	30	36	ND	ND	ND	ND
Trim25	Q61510	71.7	8.36E+06	21	24	39	1.96E+04	1	1	3
Dtx3l	Q3UIR3	83	4.62E+06	18	23	36	6.62E+04	2	2	3
Scyl2	Q8CFE4	103.3	2.37E+06	16	19	26	6.67E+05	10	10	15
Tuba1c	P68373	49.9	2.45E+06	16	36	53	8.93E+05	15	31	44
Rbck1	Q9WUB0	57.5	1.04E+06	14	14	36	ND	ND	ND	ND
Ddx17	Q501J6	72.4	1.47E+05	8	13	15	NR	7	10	12
Ubqln1	Q8R317	62	1.15E+06	8	9	18	2.29E+04	4	4	10
Mvp	Q9EQK5	95.9	2.88E+05	8	8	11	1.41E+05	4	4	6
Birc2	Q62210	69.6	4.02E+05	8	8	13	ND	ND	ND	ND

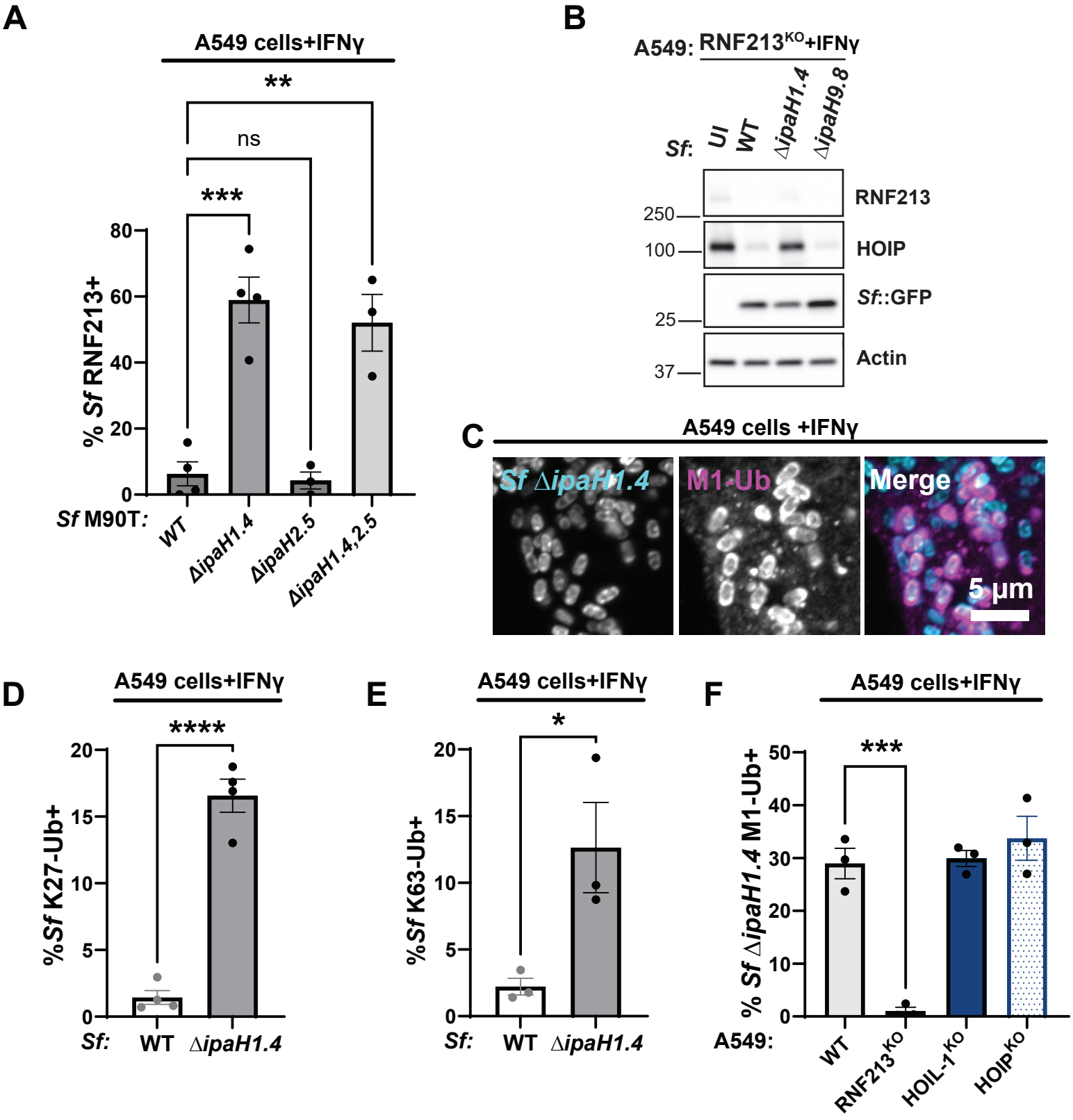
A
A549 cells+IFNγ
**
ns
***
% Sf RNF213+
80
60
40
20
0
Sf M90T:
WT
ΔipaH1.4
ΔipaH2.5
ΔipaH1.4,2.5
B
A549: RNF213KO+IFNγ
Sf:
UI
WT
ΔipaH1.4
ΔipaH9.8
250
100
25
37
RNF213
HOIP
Sf::GFP
Actin
C
A549 cells +IFNγ
Sf ΔipaH1.4
M1-Ub
Merge
5 µm
D
A549 cells+IFNγ
****
%Sf K27-Ub+
20
15
10
5
0
Sf:
WT
ΔipaH1.4
E
A549 cells+IFNγ
*
%Sf K63-Ub+
20
15
10
5
0
Sf:
WT
ΔipaH1.4
F
A549 cells+IFNγ
***
% Sf ΔipaH1.4 M1-Ub+
50
40
30
20
10
0
A549:
WT
RNF213KO
HOIL-1KO
HOIPKO

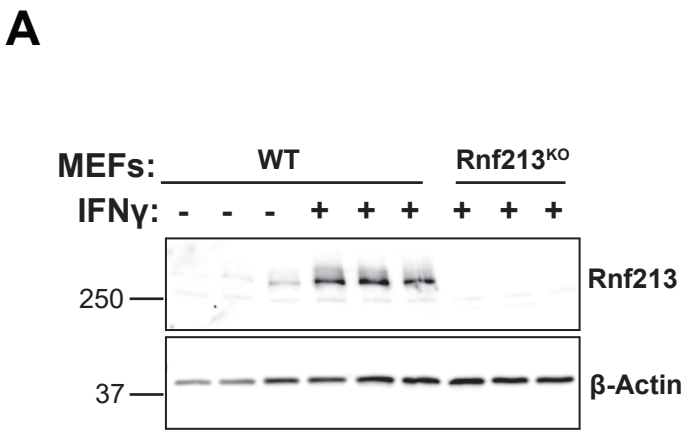
A
MEFs:
WT
Rnf213KO
IFNγ:
- - - + + + + + +
250
37
Rnf213
β-Actin

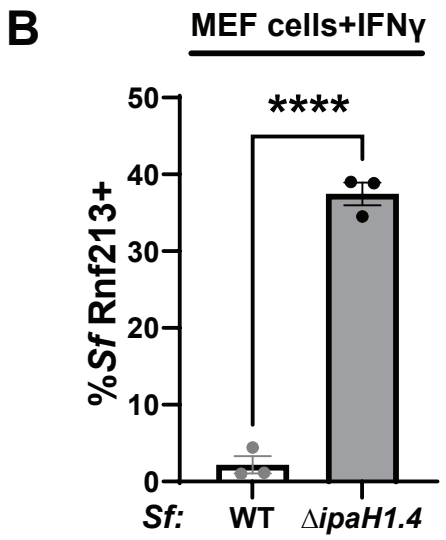
B
MEF cells+IFNγ
****
%Sf Rnf213+
50
40
30
20
10
0
Sf:
WT
ΔipaH1.4

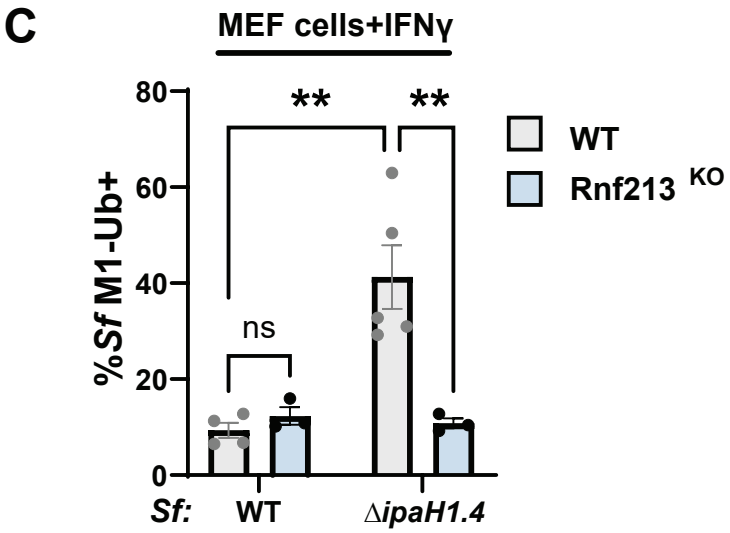
C
MEF cells+IFNγ
**
**
ns
%Sf M1-Ub+
80
60
40
20
0
WT
Rnf213 KO
Sf:
WT
ΔipaH1.4

INT-Ub Construct	Amino acid sequence (ORF)
WT	MQIFVKTLTGKTITLEVEPSDTIENVKAKIQDKEGIPPDQQRLIFAGKQLEDGS AWSHPQFEKSATLSDYNIQKESTLHLVLRLRGG
7KR	MQIFVRTLTGRTITLEVEPSDTIENVRARIQDREGIPPDQQRLIFAGRQLEDGS AWSHPQFEKSATLSDYNIQRESTLHLVLRLRGG
6KR+K6	MQIFVKTLTGRTITLEVEPSDTIENVRARIQDREGIPPDQQRLIFAGRQLEDGS AWSHPQFEKSATLSDYNIQRESTLHLVLRLRGG*
6KR+K11	MQIFVRTLTGKTITLEVEPSDTIENVRARIQDREGIPPDQQRLIFAGRQLEDGS AWSHPQFEKSATLSDYNIQRESTLHLVLRLRGG*
6KR+K27	MQIFVRTLTGRTITLEVEPSDTIENVKARIQDREGIPPDQQRLIFAGRQLEDGS AWSHPQFEKSATLSDYNIQRESTLHLVLRLRGG*
6KR+K29	MQIFVRTLTGRTITLEVEPSDTIENVRAKIQDREGIPPDQQRLIFAGRQLEDGS AWSHPQFEKSATLSDYNIQRESTLHLVLRLRGG*
6KR+K33	MQIFVRTLTGRTITLEVEPSDTIENVRARIQDKEGIPPDQQRLIFAGRQLEDGS AWSHPQFEKSATLSDYNIQRESTLHLVLRLRGG*
6KR+K48	MQIFVRTLTGRTITLEVEPSDTIENVRARIQDREGIPPDQQRLIFAGKQLEDGS AWSHPQFEKSATLSDYNIQRESTLHLVLRLRGG*
6KR+K63	MQIFVRTLTGRTITLEVEPSDTIENVRARIQDREGIPPDQQRLIFAGRQLEDGS AWSHPQFEKSATLSDYNIQKESTLHLVLRLRGG*
5KR+K27-63	MQIFVRTLTGRTITLEVEPSDTIENVKARIQDREGIPPDQQRLIFAGRQLEDGS AWSHPQFEKSATLSDYNIQKESTLHLVLRLRGG*

Table 1: Internally STREP-tagged Ubiquitin (INT-Ub) constructs. Ubiquitin lysines are shown in red. Strep tag sequence in highlighted in green